

The AH Pictoris syndrome: Continuous trains of stunted outbursts in novalike variables

ALBERT BRUCH¹

¹*Laboratório Nacional de Astrofísica
Rua Estados Unidos, 154,
37504-364 Itajubá – MG, Brazil*

ABSTRACT

Novalike variables are a subgroup of cataclysmic variables (CVs) that – unlike dwarf novae – do not exhibit strong brightenings in their long-term light curves. Variations over time scales of weeks, months or years are mostly restricted to irregular low-amplitude modulations. However, some of them occasionally suffer from so-called stunted outbursts, that is, small-scale brightenings of less than a magnitude lasting for a couple of days to weeks. There is no consensus about the physical mechanisms behind these outbursts. Here I discuss the common properties of a group of novalike variables (which I call AH Pictoris stars after its most prominent member) that exhibit a continuous train of successive stunted outbursts over their entire observational history, or at least for several years. The outburst amplitudes are stable in a given system, always ranging between 0.5 and 1 mag in the visual band. The outburst intervals, at an overall range between 12 and 30 days, and the outburst profiles can gradually evolve, but no sudden changes are observed. On shorter time scales the orbital waveforms are not only surprisingly similar, but also evolve in the same way over the outburst cycle. All AH Pic stars have absolute visual magnitudes in the overlap region between absolute magnitudes of all novalike variables and of quiescent dwarf novae above the CV period gap. So far, I identified seven novalike variables with the consistent photometric behavior which may be termed the AH Pic syndrome. Several more systems may be related objects. The relationship to the anomalous Z Cam stars is discussed.

Keywords: Stars: binaries: close – Stars: variables: general – Stars: Novae, cataclysmic variables

1. INTRODUCTION

As is well known since the development, in the 1960ies and 70ies, of a basic model, summarized in the excellent early reviews by Warner (1976) and Robinson (1976), cataclysmic variables (CVs) are interacting binary systems where a late type secondary star – in most cases on or close to the main sequence – transfers matter to a white dwarf primary. Before the matter can settle on the surface of the compact object, it forms an accretion disk around the white dwarf if no strong magnetic fields are present, or otherwise forms accretion columns or curtains, sometimes in combination with truncated disks.

Non-magnetic CVs can roughly be divided into dwarf novae that undergo semi-regular outbursts with amplitudes of $\approx 2\text{--}6$ mag and intervals ranging from days to years, and novalike variables (NLs) that do not suffer from such eruptions but remain on a rather stable long-term brightness level (except for occasional low states in the subclass of VY Scl stars). Here, I also count among the NLs most classical or recurrent novae because long

after the large-scale nova outbursts which occur in intervals of decades to millennia in these systems they behave much like NLs.

The reason for the distinct long-term photometric behavior of dwarf novae and NLs is a much lower average mass transfer rate from the secondary star in the former. The accretion disk is then in a low viscosity state and transfers less matter to the white dwarf than it receives from the late type component. Therefore, material is accumulated until a disk instability mechanism (DIM) sets in (for a review, see Lasota 2001) that elevates the disk viscosity so that the excess matter is rapidly dumped upon the primary star. This is seen as a dwarf nova outburst. Once the disk is depleted of mass, it returns to its low viscosity state, the outburst ends, and the cycle begins again. The DIM only works if the average mass transfer rate remains beneath a critical level \dot{M}_{crit} . In novalike variables it is above this limit which means that the accretion disk is always in a high viscosity state. The mass accretion rate onto the white dwarf is equal to the mass transfer rate, the disk is in a steady

state, and dwarf nova type eruptions are suppressed. In a sense NLs can thus be regarded as dwarf novae in a permanent outburst.

Of course, this is an idealized picture and should be taken *cum granum salis!* Even disregarding the low states of VY Scl stars, NLs suffer from moderate long-term brightness variations (see, e.g., the recent synoptic study of eclipsing novalike variables of Bruch 2024a). Since the brightness of CV is to a large part determined by the mass transfer rate within the accretion disk, and therefore – in NLs – by the rate at which the disk receives matter from the secondary star, modulations of their brightness can at least in part be explained by variations in the mass transfer rate. But other brightness variations may require different mechanisms, including some kind of modified DIM. Here, I am referring to small scale (amplitude: some tenths of a magnitude) brightenings, lasting for about one or two weeks observed in some NLs. They were first described in some detail by Honeycutt et al. (1998) who coined the term ‘stunted outbursts’ for these events.

Such stunted outbursts occur in general irregularly and sparsely. However, a small number of stars are known to exhibit continuous trains of such event over years. These are CM Del (Zsidi et al. 2023), FY Per (Honeycutt & Kafka 2004), V1116 Cep (Shears 2020; Shears & Bean 2023), and KIC 9202990 (Østensen et al. 2010; Ramsay et al. 2016). Some more systems are identified in this contribution. I call them AH Pic stars after the prototype that exhibits their peculiar photometric behavior most clearly. In the above mentioned papers, the respective stars were always described as isolated cases with unusual properties. They were never discussed as a group. The purpose of the present paper is to draw attention to the commonalities between the members of this group and to review existing ideas (and their problems) concerning the origin of stunted outbursts.

In Sect. 2 I present the sources for the data which form the basis of this study. Sect. 3 starts with a brief description of the common properties of the AH Pic stars. Subsequently, a characterization of the individual stars identified as belonging to this group, and of their photometric behavior is given. An analysis of the long-term properties, the absolute magnitudes, and the orbital variations of the AH Pic stars then follows in Sect. 4. Stars with stunted outbursts that are possibly related to AH Pic stars are reviewed in Sect. 5. A general discussion and a short summary conclude this work in Sects. 6 and 7.

2. THE DATA

This study is exclusively based on archival data. Light curves of all but one of the target stars were observed by the Transiting Exoplanet Survey Telescope (TESS) (Ricker et al. 2014) and were downloaded from the Barbara A. Mikulski Archive for Space Telescopes (MAST)¹. They have a time resolution of 120 sec. For a more detailed description of their structure and handling in the present context, see Bruch (2023b). In brief, I only use Simple Aperture Photometry (SAP) data because the Pre-Search Data Conditioning Simple Aperture Photometry (PDCSAP) process tends to severely distort variations on time scales longer than a few days which are crucial for this study. Data of the same objects taken in overlapping TESS sectors observed in immediate succession are combined into single light curves (referred to as LC#1, LC#2 etc.).

One of the stars, KIC 9202990, was also observed over an extended period of time as part of the Kepler space mission (Borucki et al. 2010) in long cadence mode with a time resolution of 29.4 min. During some limited intervals also light curves taken in short cadence mode with a time resolution of 59 sec are available. Both data sets (again, SAP data) are used here. They were also downloaded from MAST.

Additionally, all targets have been observed regularly during the past 10 years or so by the All-Sky Automated Survey for Supernovae (ASAS-SN) (Kochanek et al. 2017). They were downloaded from the ASAS-SN Sky Patrol website². While the survey aims to observe the entire sky once every day, even apart from seasonal gaps additional interruptions occur. Thus, the observing cadence is somewhat irregular. In the early years observations were taken in the *V* band while in more recent years the *g* band is employed.

Finally, light curves extending over several years were downloaded from the American Association of Variable Star Observers (AAVSO) International Database³ (Kafka 2021). They complement the ASAS-SN data of three targets (V2837 Ori, FY Per and V1116 Cep). Only data observed in the *V* band (or reduced to the *V* band) are used.

3. THE AH-PIC SYNDROME, IDENTIFIED GROUP MEMBERS, AND LIGHT CURVES

The defining property of AH Pic stars is a continuous sequence of small scale brightenings recurring on time scales of a couple of weeks with no or only small quiescent inter-outburst phases between them. As will

¹ <https://archive.stsci.edu>

² <https://asas-sn.osu.edu>

³ <https://www.aavso.org/data-download>

be detailed below, this behavior is either permanent, or active phases over longer time intervals (years) are interrupted by periods without this kind of activity. The intervals between brightenings are not constant, but evolve slowly over various cycles, such that longer and shorter intervals are grouped but not intermingled. The outburst shape also evolves slowly between outbursts. Other common properties of the AH Pic stars are outburst amplitudes between 0.5 and 1 mag, surprisingly similar orbital waveforms that change consistently between brighter and fainter phases, and absolute visual magnitudes in the overlap between the absolute magnitude distributions of all NLs and of dwarf novae above the CV period gap. Collectively, I refer to the peculiar properties of these stars as the AH Pic syndrome.

All objects identified as AH Pic stars are classified in widely used catalogues such as Downes et al. (2001) or Ritter & Kolb (2003) and/or in the few more detailed publications on the specific systems (see below) as nova-like variables. However, this classification is not unambiguous as other sources assign them to other possible classes. In particular, in the International Variable Star Index⁴ they are also classified as UG (dwarf nova), UGZ (Z Cam-type dwarf nova) or IW (anomalous dwarf nova; IW And-type star). The relationship of the AH Pic stars in particular to the IW And-type stars will be explored in more detail in Sect. 5.2.

The most striking and obvious manifestation of the AH Pic syndrome is observed in two long TESS light curves of AH Pic which both span about a year and are separated by a 12 months interval, plus an additional shorter light curve. They are shown in Fig. 1 (left panel). The coverage by TESS of the other stars was less intensive, but for all objects light curves from other sources (either/or Kepler, ASAS-SN or AAVSO) confirm their common properties.

So far, I could identify seven NLs which exhibit at least during extended periods of time (years) the continuous sequence of stunted outbursts that is the principle manifestation of the AH Pic syndrome. Their basic parameters and the main results of this study are summarized in Table 1. Before characterizing the AH Pic syndrome in more detail, I briefly present the seven target stars and the light curves available for analysis. I start with the prototype AH Pic.

3.1. *AH Pictoris*

Only few details are known about AH Pic (= EC 05565-5934). The star was identified as a CV

by (Chen et al. 2001) in the Edinburgh-Cape Survey and classified as a UX UMa-type cataclysmic variable. Their photometry suggested an orbital period of 0.142(2) d. This was confirmed spectroscopically by Rodríguez-Gil et al. (2007) who measured a period of 0.146(4) d. They classify AH Pic as a SW Sex star and estimate a low orbital inclination of $25^\circ < i < 37^\circ$. More recently, based on TESS data Bruch (2024b) measured a more precise period of 0.1409122(2) d.

TESS observed AH Pic extensively in sectors 1–13, 27–35, 37–39, and 61–67. There is only a single sector gap between sectors 35 and 37. Therefore, the sector 27–39 data are treated here as a single light curve. Thus, two year long light curves separated by 12 months, with a one sector gap in the second one, are available, followed by a third ≈ 220 d light curve after an interval of another 18 months.

The TESS light curves of AH Pic (Fig. 1 (left)) are characterized by the continuous series of low scale outbursts which first drew my attention to the AH Pic phenomenon. A simple visual inspection shows that whereas the outburst amplitude remains reasonably constant the intervals between outbursts and the light curve profile over the outburst cycle exhibits some variability, however, not in a random fashion. They evolve gradually on time scales longer than the outburst cycle.

The continuous series of outbursts was observed over an even longer time base by the ASAS-SN. The light curve, spanning a total of ten observing seasons, and which overlaps with the TESS light curves, is shown in Fig. 1 (right). The upper panel contains the entire light curve. The individual outbursts are resolved in the lower frames where the light curve is shown in expanded form, covering one observing season in each frame. *V* magnitudes are plotted in blue, *g* magnitudes in red. The outbursts continue over the entire time interval covered by the light curve, but it is obvious that there are periods with longer and shorter outburst intervals. Moreover, in particular during the last observing season the minima between the outbursts sometimes attain a significantly fainter magnitude than otherwise (I draw attention to the expanded magnitude scale in the bottom frame of Fig. 1). Such dips also observed in CM Del, KIC 9202990 and in particular in PS Eri (see below).

3.2. *V1116 Cephei*

V1116 Cep (also known as HS 0229+8016) was identified by Aungwerojwit et al. (2005) as a cataclysmic variable among the stars of the Hamburg Quasar Survey. They measured a spectroscopic orbital period of 0.16149(3) h. Photometric variations compatible with

⁴ <https://www.aavso.org/vsx/>

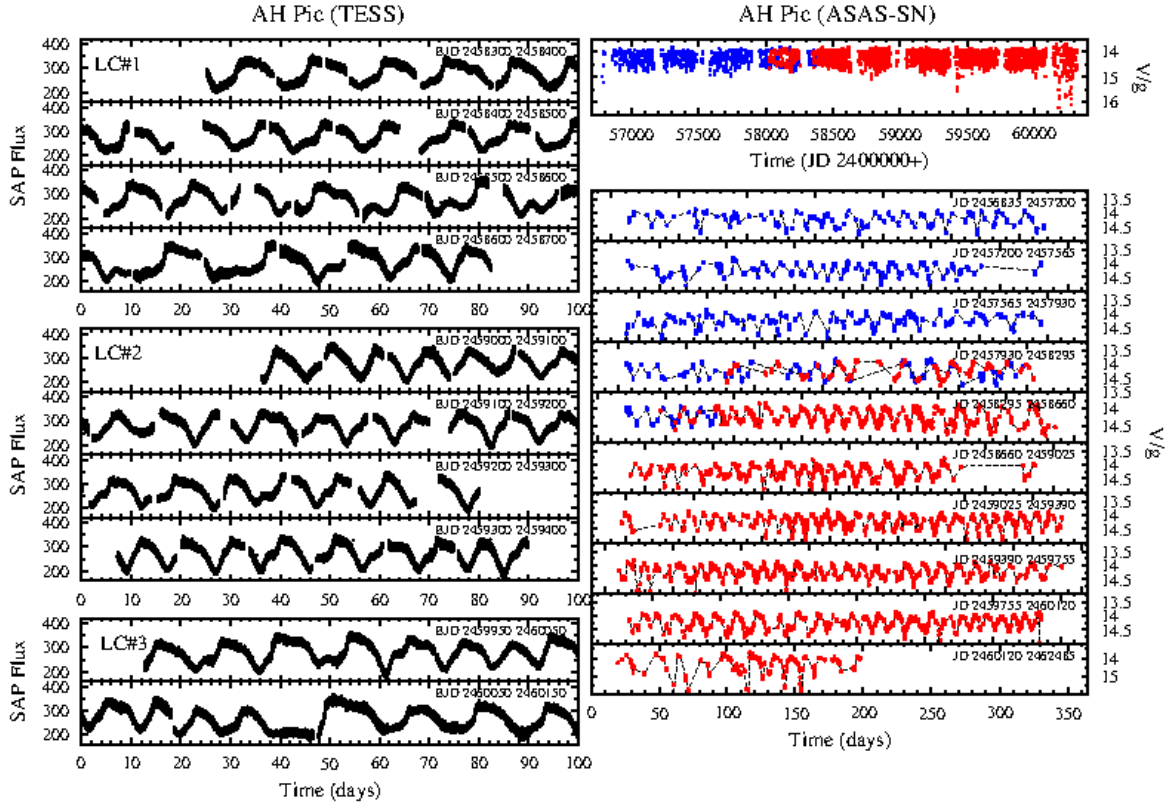


Figure 1. Light curves of AH Pic. On the left TESS data taken in sectors 1–13, 27–39 (with a gap corresponding to sector 36), and sectors 61–67, respectively, are shown. The upper panel on the right contains the full ~ 10 yr ASAS-SN light curve, while the other panels show the seasonal light curves on an expanded time scale. Blue and red dots refer to the V and g bands, respectively. Thin broken lines between the data curves are meant to guide the eye.

Table 1. Summary of the properties of AH Pic stars

Property	V1116 Cep	CM Del	PS Eri	V2837 Ori	FY Per	AH Pic	KIC 920229
orb. Period [d]	0.161439(9) ^c	0.141052(3) ^a	...	0.27610702(2) ^b	0.25837(7) ^c	0.1409122(2) ^a	0.1659404 ^d
V^e	14.25(16)	14.14(10)	13.65(16)	14.99(16)	12.80(13)	14.61(15)	15.42(19)
distance (pc) ^f	487(3)	393(3)	481(3)	650(10)	342(2)	570(5)	985(18)
$E(B - V)^g$	0.076	0.030	0.010	0.068	0.128	0.024	0.034
M_V	5.57(23)	6.07(16)	5.21(16)	5.71(33)	4.73(23)	5.76(15)	5.35(21)
light curve source ^h	T/AS/AA	T/AS	AS	T/AS/AA	T/AS/AA	T/AS	K/T/AS
median amplitude (mag)							
TESS/Kepler	0.45	0.58
ASAS-SN/AAVSO	0.59	0.51	0.95	0.98	0.65	0.66	0.83
rel. width (ampl. distr.)							
TESS/Kepler	0.12	0.17
ASAS-SN/AAVSO	0.24	0.24	0.17	0.19	0.19	0.24	0.24
median interval (d)	13.9	17.9	16.3	30.0	25.1	11.9	13.0
rel. width (interval distr.)	0.35	0.17	0.13	0.17	0.24	0.22	0.23

^a: Bruch (2023b); ^b: Bruch (2024b); ^c: Bruch (2024a); ^d: Ramsay et al. (2016); ^e: average ASAS-SN magnitude during minima (disconsidering dips); ^f: Bailer-Jones et al. (2021); ^g: Capitanio et al. (2017); ^h: T=TESS; K=Kepler; AS=ASAS-SN; AA=AAVSO

this period were also detected but did not permit to obtain a more precise value.

Here, I analyse AAVSO, ASAS-SN (Fig. 2) and TESS (Fig. 3) light curves of V1116 Cep. The AAVSO data cover well or reasonably well two time intervals. The ASAS-SN data partly overlap with the AAVSO light curve, but also cover well a time interval which is only sparsely sampled by the latter, complementing thus the AAVSO data. The AAVSO light curve has also independently been analysed by Shears (2020). A further study of the long-term variations was presented by Shears & Bean (2023). The presence of the AH Pic syndrome in V1116 Cep is clearly confirmed.

Four TESS light curves are available, three of them encompassing two sectors, but the last one covers only one sector (Fig. 3)⁵. All of them contain several brightenings. Although these TESS data are not as extensive as those of AH Pic, they also confirm the continuous outburst sequence characterizing the AH Pic stars.

I note two special features in V1116 Cyg (see Fig. 2). (1) An absence of the outburst activity occurred during a dip in the light curve between late 2016 and early 2017 (\approx JD 2457750). A similar episode may have occurred in 2012 (around JD 2456000). (2) The range of outburst intervals is much wider than in other systems. Compare, for instance, the first and the fourth panel from top of the high resolution AAVSO light curve.

3.3. *CM Delphini*

CM Del was discovered as a CV by Bond (1978). It remains a poorly studied object. Szkody (1985) presented an optical spectrum, and Lyons et al. (2001) investigated the UV spectrum. Shafter (1985) measured a spectroscopic orbital period of 0.162 d. But this is based on few and ill-distributed data points. It differs substantially from the true period of 0.14152(3) d (Bruch 2024b). Zsidi et al. (2023) noted the presence of continuous small outbursts in the long-term light curve of CM Del, but they did not draw any inferences from this observation.

TESS observed CM Del in two consecutive sectors. The combined light curve (Fig. 3) contains two brightenings of almost identical shape. This is not sufficient to identify the AH Pic syndrome in CM Del which is,

however, impressively demonstrated in the ASAS-SN long-term light curve (Fig. 4) consisting of a continuous and uninterrupted series of stunted outbursts over the nine years covered by the observations. Whereas their amplitude is in general fairly constant, two intervals in 2022 are noteworthy when CM Del drops to significantly lower magnitudes between the outbursts (note the enlarged vertical scale in the second panel from the bottom in Fig. 4).

3.4. *PS Eridani*

The ROSAT X-ray source 1RXS J022917.1-395851 (= PS Eri) (Voges et al. 2018) is a poorly investigated object. The only dedicated study was published by Hümmerich et al. (2014) who classified the system as a VY ScI-type novalike variable. Based on SWASP data (Drake et al. 2009) they found a period of 0.136621 d in the first part (2006 observing season) of this light curve, and in 2007 after a gap of 240 d, the simultaneous presence of the same period plus a period of 0.137206 d. They speculate that the two periods may be due to orbital modulations plus a superhump. However, their findings are wrong. The two parts of the SWASP light curve have approximately the same length. Thus, their power spectra should have a similar resolution. But the right panel of Fig. 3 of Hümmerich et al. (2014), supposed to contain the power spectrum of light curve part 2 and showing both periods, has a much higher resolution than the left panel (part 1). This suggests that the right panel is based on the combined data, not only part 2. To confirm this suspicion I used the same SWASP data. The three panels of Fig. 5 show the power spectra of part 1 (2006, left), part 1+2 (2006+2007, middle) and part 2 (2007, right). It is obvious that part 1 only contains the 0.136621 d and part 2 only the 0.137206 d period. Assuming one of them to be orbital and the other one due to a superhumps leads to a superhump excess of 0.0043, much too small for either a positive or a negative superhump (Bruch 2023b). However, considering that the exact periods of superhumps in novalike variables are known to be slightly variable, and that they may be active even if no orbital variations are seen (Bruch 2019, 2023a,b), both signals may be caused by superhumps (either negative or positive). The VY ScI classification of PS Eri is mainly sustained by a deep minimum seen in Siding Spring Survey data (see Fig. 1 of Hümmerich et al. 2014).

The relationship of PS Eri to the AH Pic stars is already hinted at in the SWASP data of 2007, but the sequence of stunted outbursts is not clearly seen in later years (Figs. 1 and 2 of Hümmerich et al. 2014). The ASAS-SN light curve (Fig. 6) shows that only during

⁵ Based on the quite different aspect of the first and second TESS light curve, Shears & Bean (2023) suspect that a significant change of the behavior of V1116 Cep has occurred in the interval between them (see their Fig. 3). However, this is not the case. No significant differences are seen in Fig. 3. The apparent change of behavior mentioned by Shears & Bean (2023) can be explained by their use of PCDSAP data which contain serious distortions in particular in the second light curve (see Sect. 2).

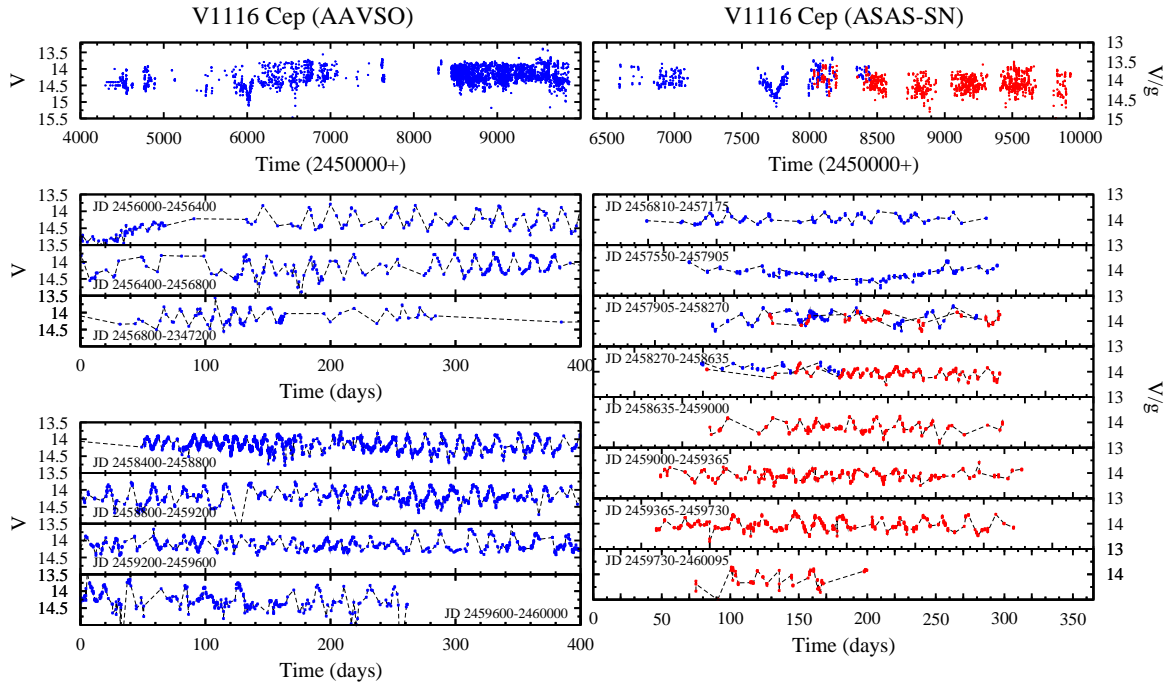


Figure 2. AAVSO and ASAS-SN light curves of V1116 Cep, structured in the same way as Fig. 1.

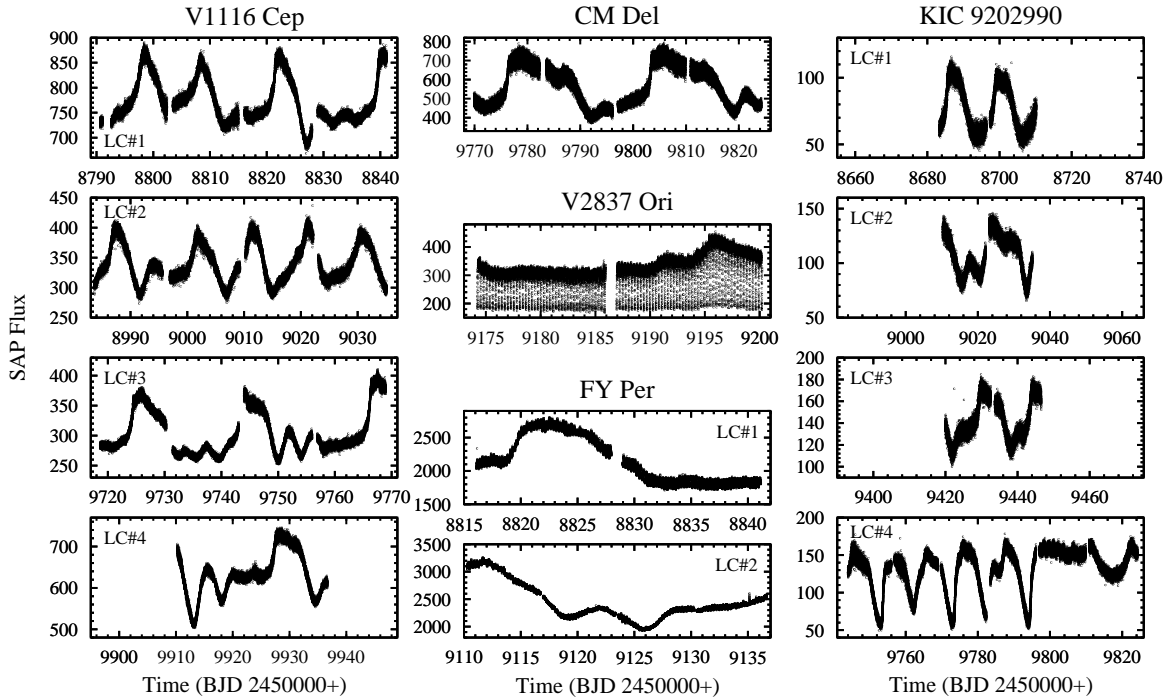


Figure 3. TESS light curves of V1116 Cep, CM Del, V2837 Ori, FY Per, and KIC 9202990.

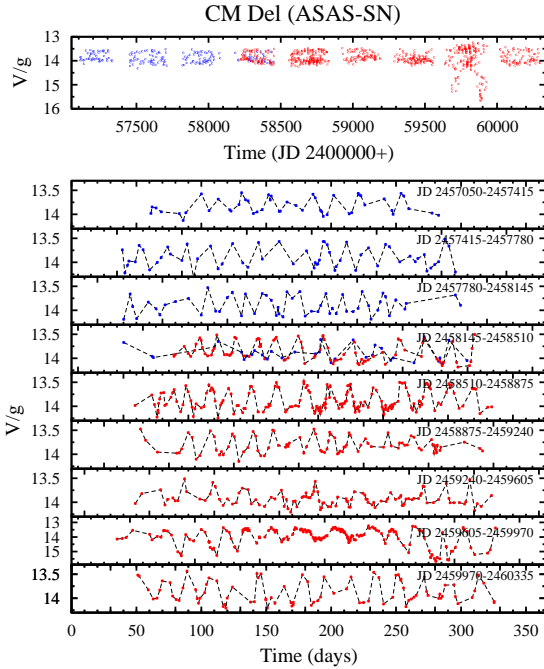


Figure 4. ASAS-SN light curve of CM Del, structured in the same way as the right side of Fig. 1.

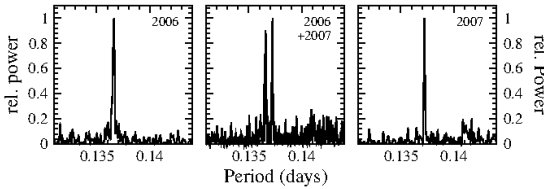


Figure 5. Power spectra of the SWASP light curve of PS Eri of the (from left to right) the 2006, the 2007+2007, and the 2007 observing seasons in a narrow range around a short term period possibly caused by superhumps with a slightly different frequency in the two seasons.

the 2018, July, the continuous train of stunted outbursts defining the AH Pic syndrome starts and continues until the end of the light curve. It is striking that more often than other AH Pic stars PS Eri exhibits deep dips between outbursts. Moreover, even before the AH Pic behavior sets in the system undergoes rather strong but irregular variations (JD 2457560–2457830), while it is quite constant in the preceding observing season.

3.5. *V2837 Orionis*

Discovered as a variable star a long time ago by Hoffmeister (1963), V2837 Ori (= NSV 1907) remained largely unstudied until recently, when Hümmerich et al. (2017) identified it as a deeply eclipsing novalike cataclysmic variable, possibly of the SW Sex subclass. The eclipses permit to measure an accurate orbital period of 0.27610702(2) d (Bruch 2024a). Thus, V2937 Ori

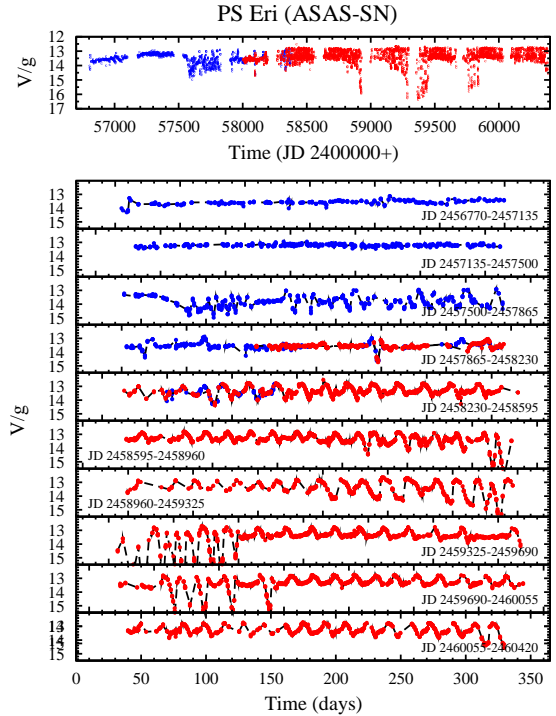


Figure 6. ASAS-SN light curve of PS Eri, structured in the same way as the right side of Fig. 1. In the lower frames some deep dips in the light curve are truncated.

is on the longer side of the CV period distribution. Hümmerich et al. (2017) also observed a 4.2 d modulation which they interpret as the nodal precession period of an accretion disk and which they used to predict a period of 0.2591 d for a (negative) superhump. An analysis of the TESS data by Bruch (2023a) confirmed the presence of superhumps.

The single sector TESS light curve of V2837 Ori (Fig. 3) only contains a single brightening and possibly the end of the decline from another outburst right at the beginning. This can only suggest the presence of the AH Pic syndrome that is, however, confirmed by the AAVSO and ASAS-SN light curves. Structured in the same way as Fig. 1 they are shown in Fig. 7. In the high resolution version, data points in a phase range of ± 0.1 around the eclipse minima as calculated using the ephemeris of Bruch (2024a) were removed in order to better visualize the continuous outburst activity. The densely covered part of the AAVSO light curve in the 2019 – 2021 observing seasons clearly shows the continuous train of small outbursts which defines the AH Pic syndrome. However, the longer time base of the ASAS-SN data reveals that the latter only started in late 2016, being absent in the three preceding observing seasons. It then persists to the end of the available data in 2023.

Thus, the AH Pic type behavior is not permanent in V2837 Ori.

3.6. *FY Persei*

FY Per is a poorly studied object. No time resolved spectroscopy has been published, and photometric studies are limited to its long-term behavior. In fact, even its CV nature was questioned (see [Downes et al. 1995](#), for a short discussion), but this issue appears to have been resolved (see, e.g., [Honeycutt 2001](#)). [Bruch \(2023b\)](#) detected negative superhumps in TESS light curves of FY Per. At 0.25837 d, he also measured the most precise orbital period.

Two TESS light curves of FY Per are available. Each one encompasses only a single sector. Both light curves (Fig. 3) contain a complete or a partial brightening. Stunted outbursts have been observed in FY Per before. First mentioned by [Sazonov & Shugarov \(1992\)](#), many more were seen by [Honeycutt \(2001\)](#). [Honeycutt & Kafka \(2004\)](#) mention the ‘common occurrence of 0.6 mag oscillations with a characteristic interval of 20–25 days’. The continuous presence of stunted outburst and thus the AH Pic syndrome is beautifully confirmed by the extensive data sets of ASAS-SN and AAVSO (Fig. 8). The AAVSO light curve covers the time interval between 1990 and 2019, but only between 1992 and 2003 it has a dense enough coverage to clearly reveal the successive train of outbursts. Complementing these data, the ASAS-SN light curve covers the more recent years between 2015 – 2023. As in AH Pic there are periods of longer and shorter outburst intervals, but overall, they are considerably longer than in AH Pic.

3.7. *KIC 9202990*

In a limited amount of early Kepler observations [Østensen et al. \(2010\)](#) noticed that the light curve of KIC 9202990 is dominated by long term variations superposed upon regular variations with a period of 0.166 d. They classified the system as a novalike cataclysmic variable and interpreted the 0.166 period as orbital. Based on the entire Kepler data set of KIC 9202990, [Ramsay et al. \(2016\)](#) investigated the system further and concluded that the long-term variations constitute a continuous train of stunted outburst (i.e. the AH Pic syndrome). Short term (flickering) variations in KIC 9202990 were studied by [Bruch \(2022\)](#)

Kepler observed KIC 9202990 for more than four years almost continuously in long cadence mode. During three limited time intervals within these four years short cadence light curves are also available (see Fig. 5 of [Bruch 2022](#)). The full long cadence light curve, reproduced in Fig. 9 (left), is a most impressive example of the AH Pic type behavior.

The temporal coverage of KIC 9202990 by TESS is much less extensive. TESS observed the star on four occasions (Fig. 3), three times during a single sector, while the last visit encompassed three sectors. A peculiarity of the latter light curve is the cessation of the outburst activity at the end. The existence of intervals without the usual brightenings is also observed in the ASAS-SN light curve (Fig. 9, right), which starts after the end of the Kepler observations and extends to the present day. It thus nicely complements the close coverage of KIC 9202990 by Kepler. Finally, just as other AH Pic systems, sometimes the minimum between outbursts attains significantly fainter magnitudes than usual.

4. PROPERTIES OF THE AH PIC STARS

4.1. *Outburst intervals and amplitudes*

The long available light curves of the target stars permit the determination of the outburst intervals (or the outburst recurrence time) and their amplitudes. To this end, I employ the ASAS-SN and AAVSO data of all systems, as well as the long cadence Kepler light curve of KIC 9202990 and the TESS light curves of AH Pic. The TESS data of the other systems are too sparse for statistically meaningful results.

Given the quite different sampling of the TESS and Kepler data on the one hand, and the ASAS-SN and AAVSO data on the other, slightly different approaches were adopted. In order to remove orbital variations and random modulations such as flickering, the TESS and Kepler data were first smoothed with a Savitzky-Golay ([Savitzky & Golay 1964](#)) filter with a cutoff time scale of 2 d and a fourth order smoothing polynomial. This reduces the impact of orbital variations on the outburst amplitude. The smoothed light curves were transformed from the flux to a magnitude scale with an arbitrary zero point. The epochs of individual maxima and minima of each outburst cycle were then measured. The average of the time intervals between subsequent maxima and subsequent minima is taken as the outburst recurrence time. Similarly, the amplitude was measured as the magnitude difference between a light curve minimum to the next outburst maximum, and again from maximum to the next minimum.

To measure outburst intervals and amplitudes in the ASAS-SN and AAVSO light curves, only those parts were used where a continuous train of outbursts could clearly be identified. The time resolution of these data is, of course, much inferior to that of the TESS and Kepler data. Therefore, a minimum or maximum point in the light curve may be somewhat different from the true minimum or maximum. This will enhance the scatter of the time interval between outburst, but should not

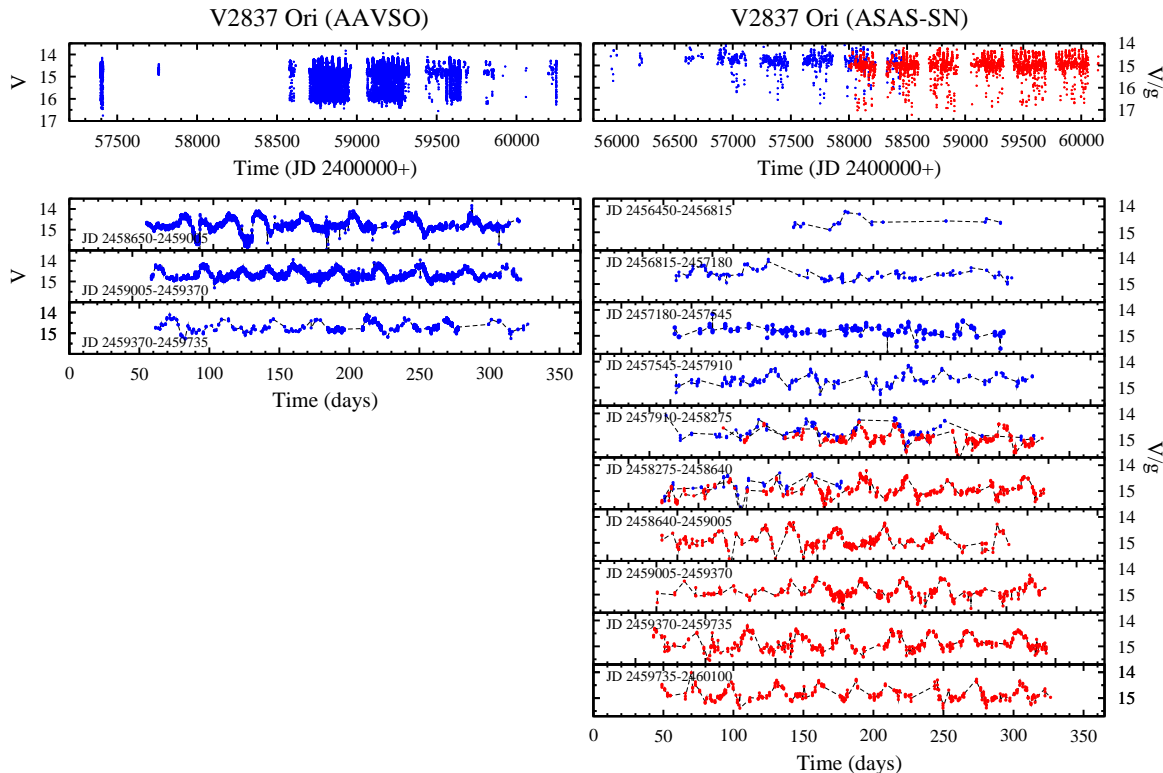


Figure 7. AAVSO and ASAS-SN light curves of V2837 Ori, structured in the same way as Fig. 1. In the high time resolution versions of the light curve the eclipses have been removed.

affect its mean or median value significantly. However, the amplitude will have a systematic error, being smaller than it really is. This effect may be somewhat compensated by random effects such as measurement errors, flickering and irregularly sampled orbital variations because on average these will push the extrema to more extreme values. In comparing the amplitude derived from the ASAS-SN or AAVSO to those of the Kepler or TESS light curves the different passbands must also be considered. While the terrestrial observations were all taken in the V or the (quite similar) Sloan g band, the TESS satellite has a wide passband between 6000 and 10000 Å, centered on the Cousins I band. Kepler has a similarly broad passband, but offset by roughly 1000 Å to the blue.

The median outburst amplitudes and intervals are listed in Table 1. I prefer to quote the median instead of the mean values because of the sometimes skewed distribution of individual outburst intervals and amplitudes. The distribution functions are shown in Fig. 10. They extend over a wide range of typically 1.5 times the median value. In order to parameterize their width the standard deviation of a Gaussian fitted to the distribution function, divided by the median value (thus, the relative width), is also listed in Table 1. Most of the amplitude distributions have an extended tail towards

high amplitudes. This reflects the fact that the light curves sometimes drop to an unusually low minimum after an outburst. This is seen at the end of the AH Pic and CM Del light curves in Figs. 1 and 4, respectively, and most clearly in the PS Eri light curve (Fig. 6). At the longer wavelengths observed by TESS and Kepler, the amplitude is significantly smaller than in the visual range (ASAS-SN and AAVSO). This can probably be attributed to the stronger contribution to the total light of the late type secondary star in the red and/or a spectral energy distribution of the outbursting light source that is bluer than the quiescent light. Most of the amplitude distributions have a single maximum. But in V1116 Cep it appears to be bi-modal. A bi-modal distribution is also suggested in the outburst intervals of AH Pic and PS Eri. Otherwise, the overall interval distributions are fairly Gaussian in shape. However, as mentioned above, variations of the outburst interval do not occur randomly but there may be periods with systematically longer or shorter intervals.

The ASAS-SN and AAVSO data are not well enough sampled to permit a reliable statement on the outburst shape. Regarding the TESS and Kepler light curves it appears that there is a continuum of shapes even in a given system that at one extreme consists of a steep rise to maximum, followed by a slowly declining plateau, and

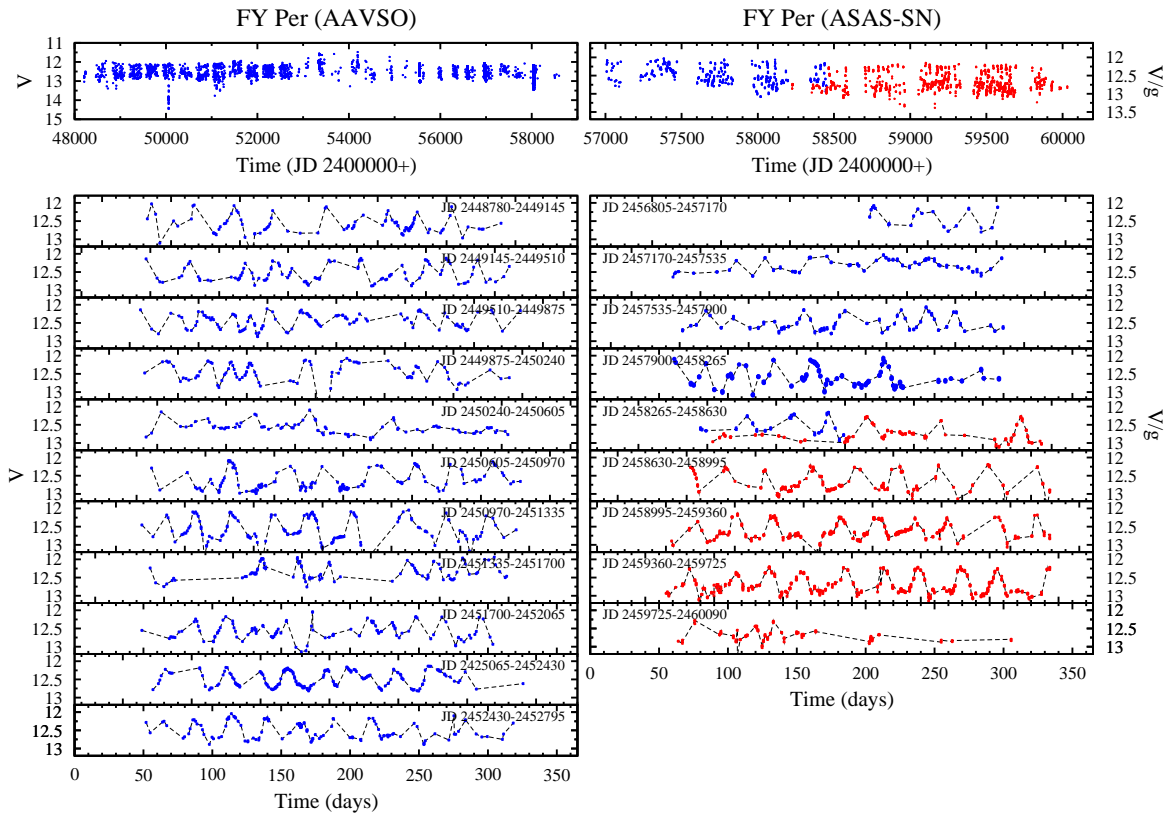


Figure 8. AAVSO and ASAS-SN light curves of FY Per, structured in the same way as Fig. 1.

then by a more rapid decline (but less so than the rise) ending the outburst. The duration of the plateau is not constant but may shrink, until at the other extreme it disappears altogether and the decline towards minimum starts right after the maximum. Just as in the case of the outburst intervals the transition between these extremes occurs only gradually over several outburst cycles. Moreover, there appears to be a positive correlation between the length of the plateau phase and the outburst interval.

4.2. Absolute magnitudes

In order to compare the absolute magnitude of the target stars with those of other novalike variables (and old novae) and with dwarf novae the average V - and g -band magnitudes of the minima between stunted outbursts (disconsidering obvious dips below the normal minima) were determined in all ASAS-SN light curves. In order to reduce the g band magnitudes to the V band, the difference between the average g and V values in the overlap region of the two band in the ASAS-SN light curves

was subtracted from all g band magnitudes⁶. Distance measurements based on Gaia DR3 data were taken from Bailer-Jones et al. (2021). Together with the interstellar absorption calculated using the reddening E_{B-V} estimated in the tri-dimensional Stilims extinction maps (Lallement et al. 2014; Capitano et al. 2017) these yield the absolute visual magnitude M_V of the AH Pic stars as listed in Table 1. Distribution functions of the absolute V band magnitudes of novalike variables (including also old novae in the sample) and dwarf novae during quiescence and outburst maximum were determined as detailed in Appendix A. Only SS Cyg- and Z Cam-type dwarf novae were considered, avoiding the on average much fainter short period SU UMa- and WZ Sge-type stars.

The distribution functions are show in Fig. 11. The absolute magnitudes of the AH Pic stars are indicated as blue bars. They are all fainter than the average $M_V = 4.42$ of novalike stars, and brighter than the average $M_V = 6.85$ of dwarf novae, lying in the overlap region between the two distribution functions.

⁶ This did not work for FY Per because the overlap is small and no outburst g magnitudes were measured. Therefore, in this case the difference between V and g averaged over the entire light curve was used.

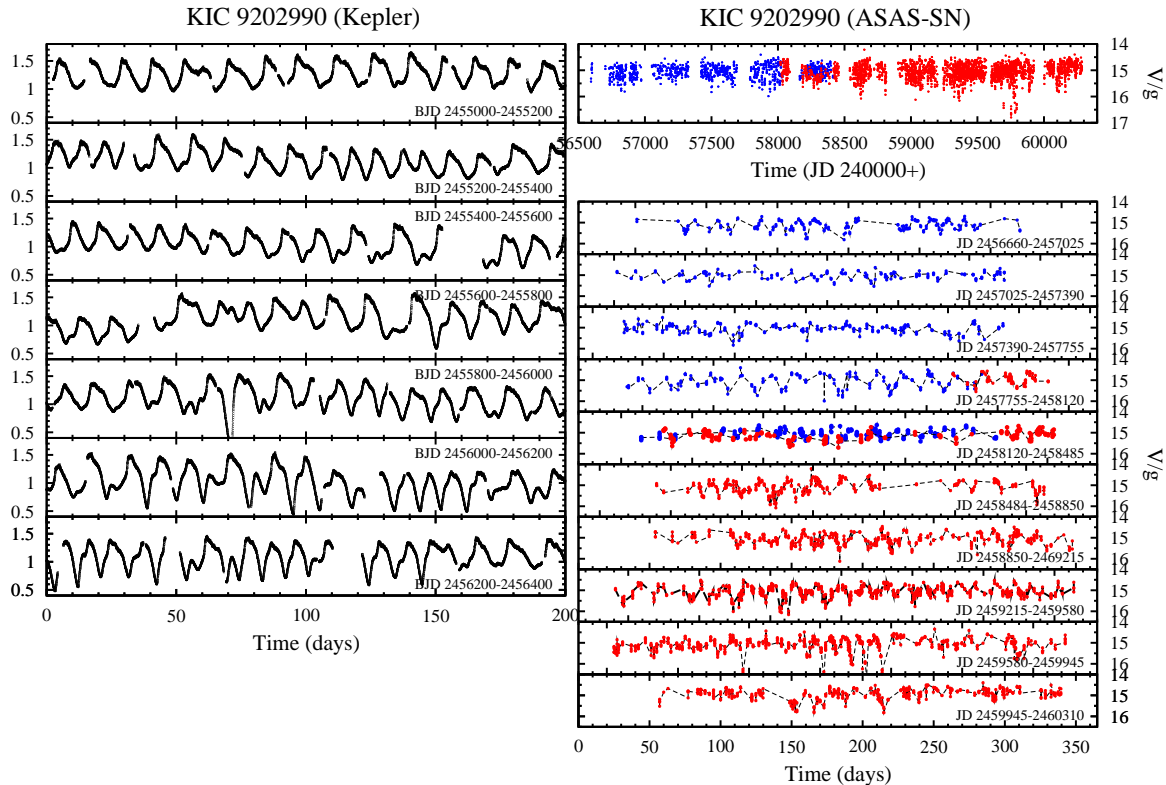


Figure 9. Kepler long-cadence light curve of KIC 9202990 (left) and its ASAS-SN light curve (right) structured in the same way as the right side of Fig. 1.

4.3. Orbital variations

The high time resolution of the TESS and Kepler data, available for all target stars except PS Eri, permits to study their variability on orbital time scales. As will be seen, the AH Pic stars share some common properties also concerning their variations around the binary orbit. The orbital periods of all the stars are listed in Table 1. The improved value for FY Per is based on the frequency of the power spectrum peak of TESS LC#2 shown in Fig. 15 of Bruch (2023b).

The accurately known orbital periods permit to construct high quality orbital waveforms. To this end, the pre-whitened light curves (that is, after subtraction of its smoothed version; see Sect. 4.1) were folded on the orbital period. To reduce the noise the waveforms were binned into intervals of width 0.01 in phase. This was done for each TESS light curve and, in the case of KIC 9202990, for the short cadence Kepler light curves⁷. As mentioned by Bruch (2023b), instead of orbital variations only a strong negative superhump is visible in TESS light curve LC#1 of FY Per. In contrast, LC#2 exhibits orbital variations along with su-

perhumps. Therefore, only the latter is suited to study the orbital waveform of FY Per.

In all systems with more than one light curve the individual data sets yielded identical results. Thus, the waveforms are stable over time and the average for these stars was constructed, weighting each light curve according to the number of contributing data points. The results are shown in Fig. 12 as black graphs. The zero point of phase is defined as the maximum of the prominent hump in the waveforms of all targets, except in the case of the eclipsing system V2837 Ori, where the center of the eclipse is taken as phase zero.

However, the average waveforms over the entire light curves are misleading. Significant details depend on the outburst phase. This is shown in Fig. 13 at the example of the two long TESS light curves of AH Pic displayed as black graphs in the two frames of the figure, binned in time intervals of 0.1 d. Beneath, the amplitude A of the orbital variations are shown in red (left hand scale of the figure). For each cycle, A was measured as the full amplitude of a sine fit to a section of the light curve including said cycle plus the preceding and following cycles. An alternative approach, fitting parabolae to the minima and the maxima of each cycle and determining the flux difference of their extrema yielded similar but noisier results. A strict correlation is observed be-

⁷ The long cadence data yielded an identical but noisier orbital waveform and are therefore not further considered in this context.

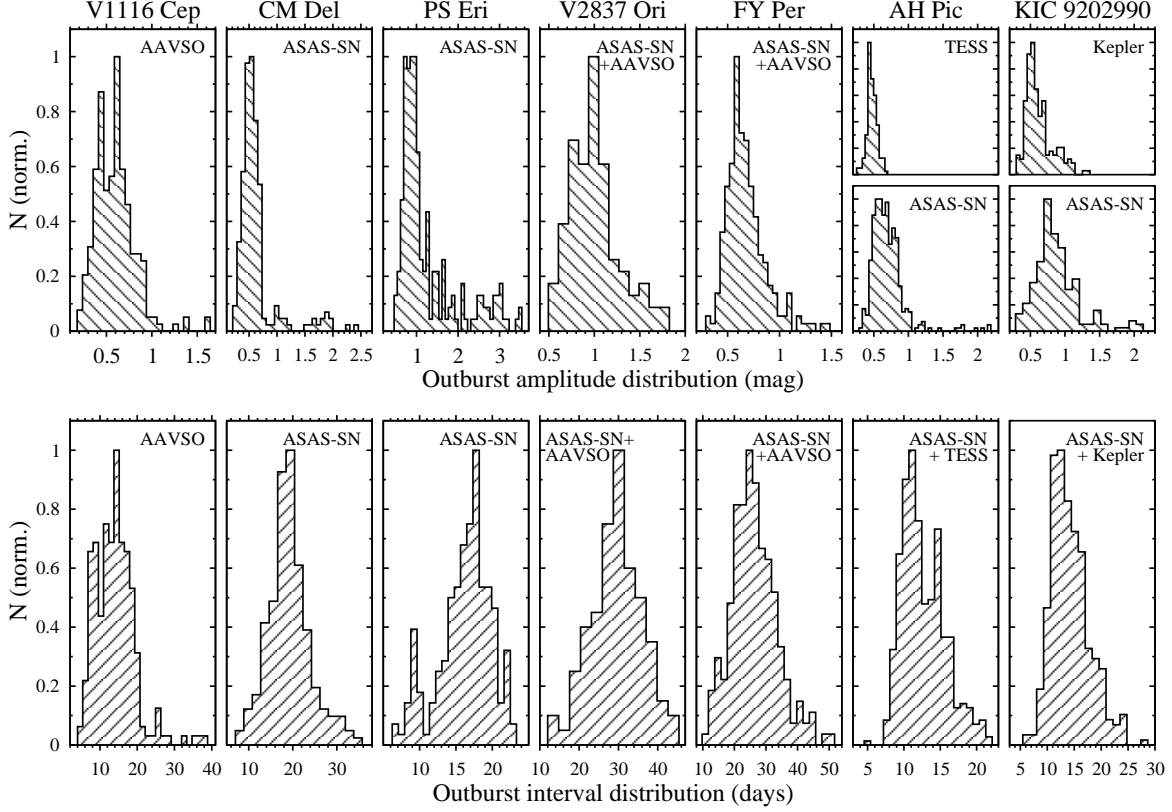


Figure 10. Distribution functions of outburst amplitudes and intervals of the AH Pic stars.

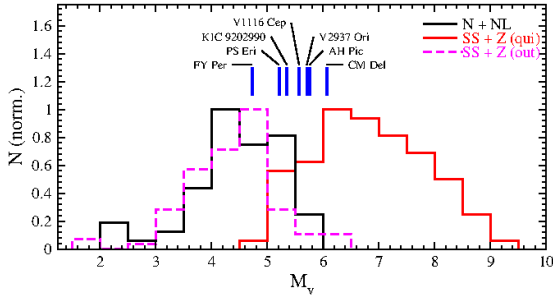


Figure 11. Distribution functions of the absolute V band magnitude of novalike variables and old novae (solid black), and of SS Cyg- and Z Cam-type dwarf novae during quiescence (solid red) and outburst maximum (dashed magenta). The blue bars indicate the absolute magnitudes of the AH Pic stars.

tween A and the brightness of AH Pic. During outburst maximum the amplitude of the orbital variations is consistently and significantly higher than during minima. It increases by a factor of 1.8 during outburst. That the amplitude of the orbital variations increases during outbursts may not be surprising, but it is also not entirely trivial. It means that the extra light during the brightenings is not just added to the inter-outburst light, but that it is also modulated around the orbit. The median outburst amplitude of AH Pic of 0.45 mag leads to a flux

ratio $F_{\max}/F_{\min} = 1.5$ between outburst maximum and minimum. This is less than the observed amplitude ratio of the orbital variations. Thus, the extra light during outburst is even stronger modulated than the quiescent light.

The blue dots in Fig. 13 show the difference $O - C$ between the observed epochs of the orbital minima, given as the time of minimum of the quadratic fit to the minima of each cycle, and the calculated epoch using the orbital period. Again, there is a clear dependence of $O - C$ on the outburst phase of AH Pic. This means that the orbital minimum is shifted to earlier phases during outburst.

In order to visualize the outburst phase dependent differences for all target stars, waveforms were constructed separately for outburst and inter-outbursts intervals. Since there is no clear distinction between these stages, they are here taken to be roughly as the upper and lower parts of the continuous outburst trains. For simplicity, I refer to the latter as quiescence, being aware that truly quiescent intervals cannot well be defined in AH Pic stars. The resulting waveforms are shown as red (outburst) and blue (quiescence) graphs, respectively, in Fig. 12 and are remarkably similar for the different objects.

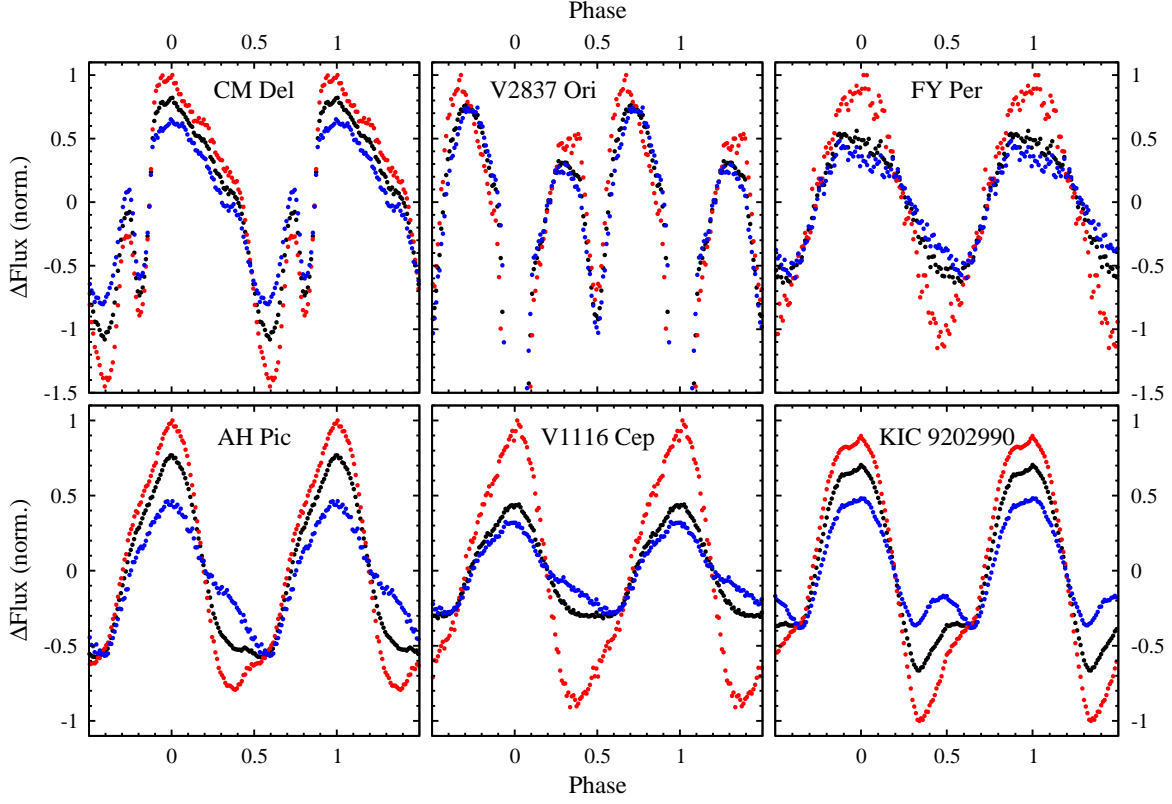


Figure 12. Orbital waveforms of the AH Pic stars. The black graphs refers to the entire light curves, the red ones to outburst, and the blue ones to inter-outburst phases.

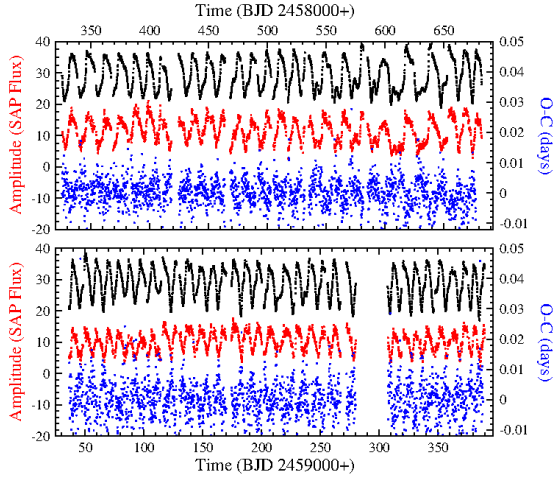


Figure 13. Dependence of the orbital variations of AH Pic on the outburst phase in light curves LC#1 (top) and LC#2 (bottom) of AH Pic. The black graphs contain the light curves, binned in time intervals of 0.1 d. The red graphs (left hand scale) show the amplitude of the orbital variations, the blue one the $O - C$ values (right hand scale) between the observed and calculated epochs of orbital minima.

In the prototype AH Pic the waveform is dominated by a single hump extending over $\approx 70\%$ of the orbit. In quiescence as well as in outburst it has a small kink at

phase ≈ 0.8 after which the gradient is slightly smaller. During quiescence, halfway down the orbital hump the slope of the waveform decreases suddenly and the flux continues to drop linearly until the onset of the next hump at phase 0.60. In contrast, during outburst the decline from the hump occurs without a break until the minimum at phase 0.37. Thereafter a somewhat structured rise, which in the first part resembles the egress from a shallow eclipse, is observed until phase 0.60 (the same phase at which the linear decline during quiescence gives way to the onset of the hump), and then the hump starts.

In almost all details this behavior is repeated in V1116 Cep. The only difference is the lack of an indication for an eclipse during outburst. The waveforms of KIC 9202990 were already shown and discussed by Bruch (2021). Again, the same pattern is observed, but the eclipse-like feature is now also present during quiescence. The difference of its minimum phase during quiescence and outburst is noteworthy. Moreover, the kink during the rising phase of the hump now occurs much closer to the hump maximum. During the brightening an additional spike develops upon the hump.

In both, outburst and quiescence, the CM Del waveform contains two well expressed minima of different

width which gives the impression of the occultation of two light sources of different extension. Notwithstanding the somewhat different shape of the orbital hump, the quiescent waveform resembles very much that of KIC 9202990 during quiescence. Moreover, just as in AH Pic and V1116 Cep there is a transition to a shallower slope (shortly before dropping into the first minimum) on the declining branch of the hump which is missing during outburst. The outburst waveform differs from that of KIC 9202990 in the sense that the second, sharper minimum is absent in the latter. The phase of the second minimum does not change between outburst and quiescence, but the phase of the first one is slightly later during outburst compared to quiescence, just as in KIC 9202990.

The FY Per waveforms are noisier because fewer data are available. But again, the pattern close to the hump minimum during both, quiescence and outburst, is the same as in AH Pic and V1116 Cep. However, at hump maximum a difference is obvious during quiescence. Concerning V2837 Ori, the interpretation of the waveform is hampered by the deep primary eclipse and also by the clear presence of a secondary eclipse. A slight difference of the phase of the maximum after the secondary eclipse is observed between outburst and quiescence. Before secondary eclipse the differences between outburst and quiescence appears to be compatible with the structure of the other AH Pic stars close to the orbital minimum, namely a rise during outburst and a slight decline during quiescence.

The consistent change of the waveform over the outburst cycle is not only a property of the average over all light curves of a given system but it repeats itself in each individual cycle. This is shown in Fig. 14 where in the upper panels a limited interval of the light curves of AH Pic and KIC 9202990 is displayed. The lower panels contain as a function of time the average orbital waveforms in a sliding window with a width of 10 cycles in a tri-dimensional representation. Orbital minima are color-coded in blue/purple, maxima in yellow/red. It is obvious that during each outburst cycle the variations of the waveform are strictly correlated with the brightness in the same way as in the average waveforms of Fig. 12.

Given the considerable variety of orbital waveforms of novalike variables in general, and their frequent variability on time scales of months and years (Bruch 2024a), their constancy, extreme similarity, and consistent variations between outburst and quiescent phases in the AH Pic stars is amazing. It points at a significant likeness of their structure and evolution during the outburst cycle, emphasizing the kinship of all AH Pic stars.

5. RELATED SYSTEMS

5.1. *Other novalike variables with stunted outbursts*

Stunted outburst in other novalike variables and old novae have been observed and are characterized in the literature, for instance by Honeycutt (2001) and Vogt et al. (2018). In some cases the authors claim that they occur frequently in quick succession. This raises the question if these stars could be related to the AH Pic stars. Most of the previous studies are based on observations sampled less frequently and/or over a smaller time base than is available in modern surveys. Thus, a better coverage may shed light on such a relationship. For 11 of the systems listed in the mentioned references useful ASAS-SN light curves exist. Others – in particular some old novae observed by Vogt et al. (2018) – are too faint for the ASAS-SN. The 11 light curves are reproduced in Fig. 15 on the same time scale. Eclipses in the eclipsing NLs UU Aqr, AC Cnc, SW Sex, and RW Tri have been removed. The uppermost frame of the figure contains the ASAS-SN light curve of AH Pic as a reference for the visual impression of a light curve with continuous stunted outbursts on the chosen horizontal scale. In all cases I have also inspected plots of the seasonal light curves on an expanded scale in order to better identify small scale outbursts.

Many of the light curves exhibit consistent brightness variations with amplitudes of the order of some tenths of a magnitude on different time scales. This makes it sometime difficult to draw a line between brightenings which deserve the name stunted outbursts and other variations. No outbursts were detected in SW Sex. With some confidence, stunted outbursts were occasionally seen in UU Aqr, CP Lac, DI Lac, HR Lyr, V841 Oph and RW Tri. But even if they sometimes occur close in time, they remain far from forming the long sequences of brightenings in immediate succession that defines the AH Pic syndrome.

AC Cnc and GI Mon show some resemblance to the AH Pic stars. Starting in the second half of 2019 AC Cnc exhibits semi-regular brightenings with amplitudes typical for stunted outbursts. But their duration and the intervals between them are somewhat longer than in the genuine AH Pic stars. Moreover, the brightenings are normally separated by a quiescent interval of appreciable length. The light curve of GI Mon contains sections of (noisy) sequences of variations with an amplitude of roughly 0.8 mag which repeat about every 50 days. There may be thus a kinship between these two systems and the AH Pic star.

X Ser is a special case. Honeycutt et al. (1998) observed three small scale outbursts in the old nova X Ser

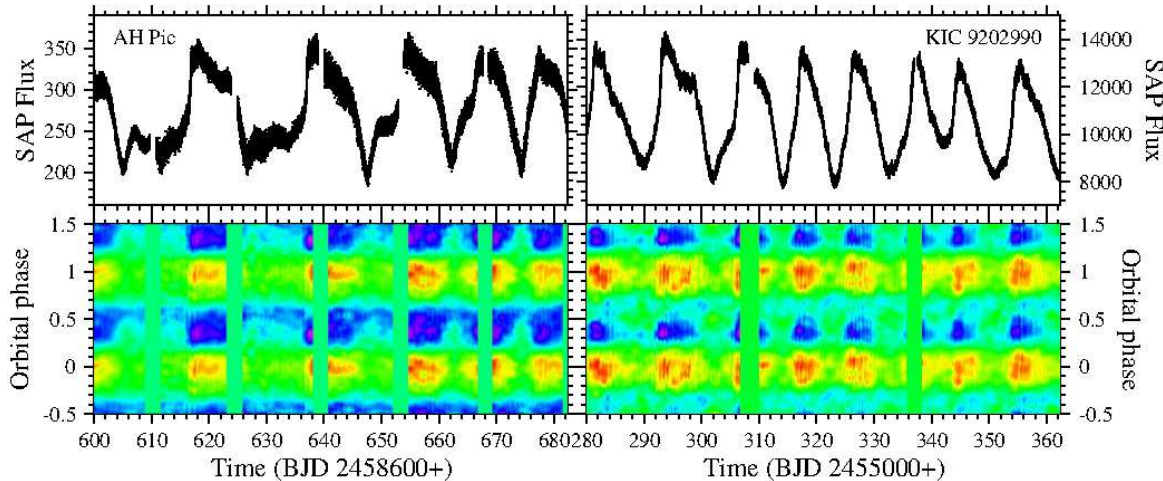


Figure 14. *Top:* Limited section of the light curves of AH Pic and KIC 9202990. *Bottom:* Average waveforms in a sliding window with a width of 10 orbital cycles as a function of time. Orbital minima are color-coded in blue/purple, maxima in yellow/red. The vertical green bars mark intervals during which the sliding window contains less than 10 cycles due to gaps in the original light curves and therefore no average waveforms were calculated.

(1903). However, the ASAS-SN light curve tells a quite different story. It is punctuated by fairly regular outbursts on a much larger scale than normal stunted outbursts. Using also AAVSO data, disregarding three outburst intervals longer than 300 d, and assuming that some outbursts have been missed, I derive an average interval between the brightenings of 241 ± 18 d, an average amplitude of 2.6 ± 0.3 mag and a mean total duration of 62 ± 5 d. The amplitude is quite normal for a dwarf nova. The comparatively long outburst interval and duration is not unusual at the orbital period of ≈ 1.5 d (Schaefer 2022) (see the discussion in Bruch 2017). Thus, a century after its eruption as a nova X Ser appears to have transformed into an ordinary dwarf nova. For a more detailed analysis of the long-term light curve of this object, see Šimon (2018).

Of all the stars of this section V794 Aql resembles the AH Pic stars most. Honeycutt et al. (2014) studied the long-term variations between 1990 and 2012 in detail, rectifying some views expressed in earlier publications. They detected stunted outbursts ‘which appear, at least sometimes, as continuous oscillations’. The ASAS-SN light curves confirms this notion. Only in the 2019 observing season (JD 2458560-2458820) the continuous outbursts are absent. V794 Aql is a well-known VY Scl star and went through a low state during that year. But even continuing in this low state for at least another 1.5 years the outburst activity was resumed in the following season. A notable difference between V794 Aql and the AH Pic stars is the much larger outburst amplitude. It is almost always well above 1 mag and can reach 3 mag during the low state. Noting that the brightness at outburst maximum remains rather constant, the

larger amplitude during the low states suggests that the intrinsic outburst properties do not change, but the outburst amplitude is attenuated by a stronger background light during the high state. Unfortunately, it is not possible to verify if the similarities between V794 Aql and the AH Pic stars extend to the orbital waveform. Although a single sector TESS light curve, containing a 1.2 mag outburst is available, its power spectrum lacks a convincing signal at or close to the spectroscopic orbital period of 0.1533 d (Honeycutt & Robertson 1998) or any other indication of a stable periodicity.

Recently, Zsidi et al. (2023) presented long term light curves of further NLs exhibiting brightenings similar to stunted outbursts. Of these, discounting FY Per and CM Del as already known AH Pic stars and the above mentioned system V794 Aql, none shows indications for the AH Pic syndrome.

5.2. Relationship to anomalous Z Cam stars

Another group of stars with some resemblance in their long-term light curves to the AH Pic stars are the anomalous Z Cam-type systems. As is well known, Z Cam stars are dwarf novae that after an outburst occasionally remain at an intermediate brightness level for an unpredictable time before returning to the quiescent state. As first noticed by Simonsen (2011), in the anomalous Z Cam stars – a term introduced by Szkody et al. (2013) – the standstills are instead terminated by another outburst. Kato (2019), who dubbed these systems IW And stars after their prototype, provided a quite specific definition for the IW And phenomenon, namely a sequence of “standstill – brightening – damping oscillation”. However, soon afterwards Kimura et al. (2020b) introduced a much broader defi-

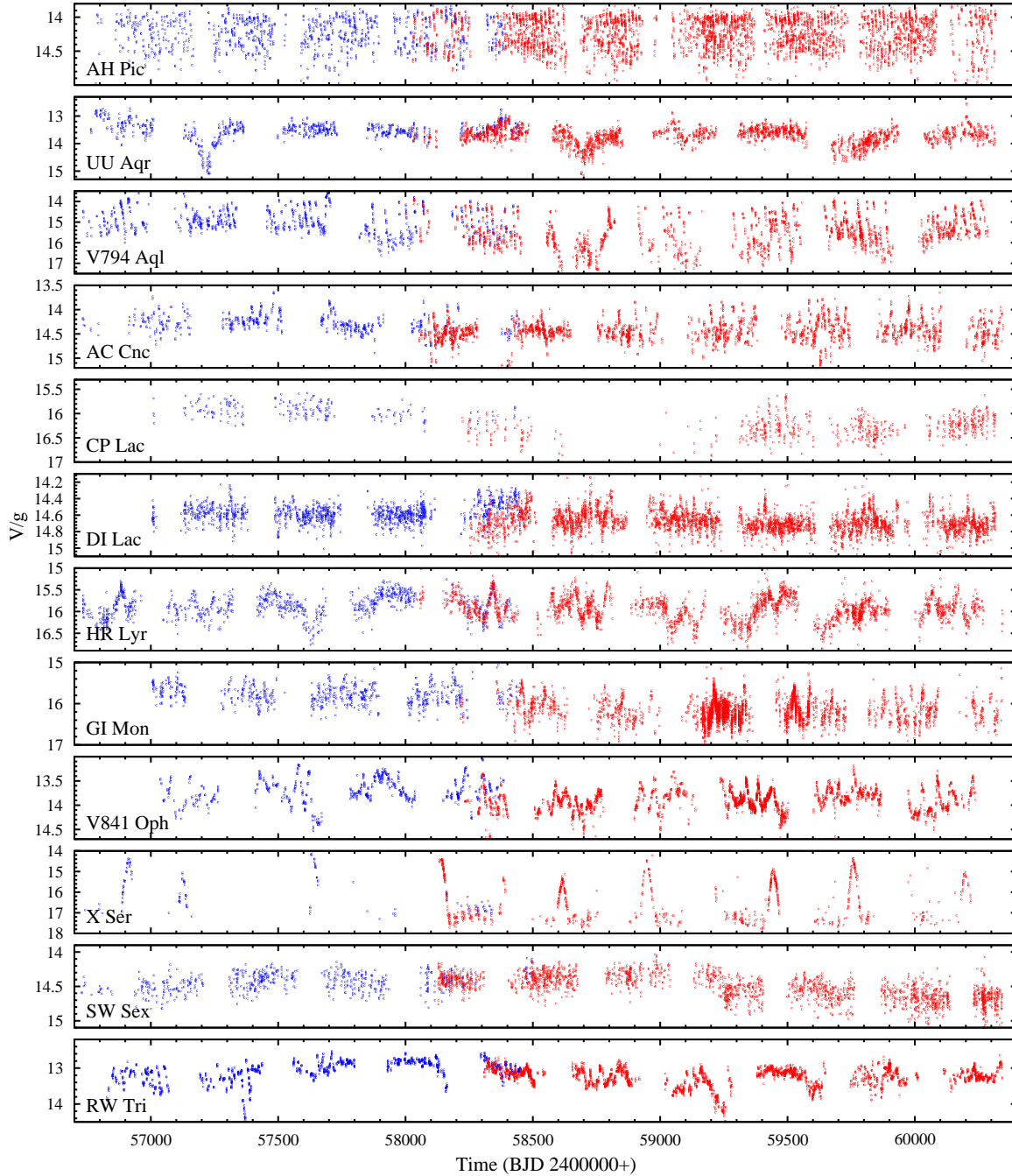


Figure 15. Synoptic view of ASAS-SN light curves of NLs with stunted outbursts reported in the literature. As a reference for the aspect of a AH Pic star light curve on the chosen horizontal (time) scale, the AH Pic light curve is reproduced in the upper frame. Blue dots represent data in the V band; g band data are shown in red.

nition, saying “it is another essential feature of the light variations in IW And stars that they would alternate in one object between the IW And-type phenomenon, Z Cam-type standstills, normal dwarf nova outbursts and heartbeat oscillations on time scales of $\sim 100 - 1000$ days”, opening the door to classify many more systems as IW And stars than the much narrower original definition. Considering the lack of well-expressed standstills

and damping oscillations, the AH Pic stars do not fit the definition of Kato (2019), but may fit into the broader definition of Kimura et al. (2020b) since the continuous sequence of small outbursts can be equated to what they call “heartbeat oscillations”. A detailed comparison between the properties of AH Pic stars and IW And stars is therefore appropriate.

I identified in the contemporaneous literature 14 systems classified as IW And stars. They are listed together with the AH Pic stars in Table 2, where the most relevant references are cited in the last column. Several more (the AH Pic star V2738 Ori among these) are mentioned in footnote 11 of Lee et al. (2021). But since these are not well documented I will ignore them here.

Because in two systems classified as IW And stars – IM Eri (Armstrong et al. 2013) and KIC 9406652 (Gies et al. 2013) – negative superhumps (nSHs) had been observed, Kimura et al. (2020b) tried with mixed success to explain their properties within a tilted disk scenario. An assessment of the presence of nSHs in all IW And and AH Pic stars based on information scattered in the literature and in TESS and Kepler data downloaded from MAST showed that in about half of the members of both types nSHs have been seen at some time or the other, but in no case are these permanent⁸ (second column of Table 2). Moreover, there is no correlation between time intervals with active nSHs and the occurrence of the IW And phenomenon or the AH Pic syndrome. The power spectra of the TESS light curves of some of the anomalous Z Cam stars contain noteworthy features not directly related to the topic of this study. These are briefly presented in Appendix B.

Phenomenologically, the light curves of anomalous Z Cam stars differ from AH Pic type light curves in two major aspects: (1) There is almost always an appreciable quiescent (or standstill) interval between outbursts, while stunted outbursts in AH Pic stars occur in immediate succession or almost so, and (2) most of the time they exhibit a dip after the outburst, while this is rather the exception in AH Pic stars.

In order to quantify these issues, the length of the standstill or quiescent intervals and the outburst durations were measured in the long-term ASAS-SN light curves (AAVSO, TESS and Kepler light curves for V1116 Cep, AH Pic and KIC 9202990, respectively) of all IW And and AH Pic stars⁹. Due to the sometimes insufficient sampling of these data sets it is not always easy to define the start and end points of these intervals or of the outbursts. Moreover, frequently it is not evident whether an more modest initial increase in brightness, before a steeper rise sets in, should be regarded as part of the outburst or as part of the preceding stand-

still. Another concern are successive local minima after an outburst, more often seen in IW And stars than in AH Pic systems (“damping oscillations”). Should these be considered as part of the inter-outburst (standstill) intervals or not? Such problems render an unbiased determination of the duration of quiescent and outburst phases difficult. However, I tried to apply the same definition to all light curves so that systematic errors should be similar in all systems and the results should at least roughly be comparable.

Similarly, the definition of dips after outbursts is somewhat subjective. Here, I consider as dips only minima that have a depth beneath the quiescent or standstill magnitude level similar or larger than the average outburst amplitude, that is, minima similar to those occurring during the last but one observing season of CM Del (upper panel of Fig. 4) or occasionally seen in PS Eri (Fig. 6). Not unfrequently, in some IW And stars such deep dips occur after successive brightenings without preceding standstills. During such intervals the outburst activity is indistinguishable from normal dwarf nova behavior with rapidly repeating outbursts. Here, they are not considered to be part of the IW And activity.

The average ratio between the outburst duration and the duration of an entire quiescence (standstill) – outburst cycle is the outburst duty cycle listed in column 3 of Table 2. Column 4 contains the fraction of brightenings that are followed by a dip in the light curve. Concerning both criteria there is a rather clear distinction between AH Pic stars and IW And stars. In the former group the outburst duty cycle is much higher and varies over a smaller range than in the latter. The contrast between the groups concerning the fraction of dip occurrences is just as striking. There is only one outlier among the IW And stars. ASAS J071404+70043 has a high duty cycle, and the dip occurrence rate is low. This is the normal behavior of AH Pic stars. Therefore, this system should better be considered as a AH Pic star instead of a IW And star.

There are thus quantitative differences between both groups of stars. Additionally, the AH Pic stars form a significantly more homogeneous group compared to the anomalous Z Cam stars, spanning a much smaller parameter range. While some ideas about the mechanism causing the IW And phenomenon float in the literature (Hameury & Lasota 2014; Kimura et al. 2020a,b) this question cannot be considered as solved. The reasons for the AH Pic syndrome are equally unknown (see Sect. 6). Unless the qualitatively similar, although quantitatively distinct phenomenological behavior of the two groups can eventually be traced to different physical processes the possibility of a close relationship between them re-

⁸ No observations suitable for the detection of superhumps are available for PS Eri and BO Cet. The long TESS light curves of Karachurin 12 almost always contain nSHs, except for short time intervals.

⁹ Since no suitable long-term light curve of BC Cas is available, the short light curve reproduced by Kato et al. (2020) was used for a rough estimate.

Table 2. Comparison between the properties of AH Pic stars and IW And stars

Name	nSH ^a	Duty cycle ^b	Dip occurrence ^c	Ref ^d
AH Pic stars				
V1116 Cep	+	0.90	0.02	1
CM Del	–	0.96	0.06	1
PS Eri	?	0.88	0.17	1
V2837 Ori	+	0.77	0.05	1
FY Per	+	0.90	0.03	1
AH Pic	–	0.90	0.03	1
KIC 9202990	–	0.90	0.01	1
IW And stars				
IW And	–	0.43	0.74	2
BC Cas	–	0.35	0.33	3
V513 Cas	+	0.45	0.23	2
BO Cet	?	0.64	0.42	4
ST Cha	–	0.48	0.78	5
V507 Cyg	+	0.61	0.28	6,7
IM Eri	–	0.34	0.90	7,8
V523 Lyr	+	0.33	0.38	9
HO Pup	–	0.57	0.33	10
FY Vul	+	0.64	0.28	6
LAMOST J065237.19+243622.1	+	0.60	0.10	11
ASAS J071404+7004.3	+	0.87	0.02	12
KIC 9406652	+	0.33	0.56	13,14
Karachurin 12	+	0.65	0.03	15

^a: negative superhumps occurrence: + (sometimes), – (never)

^b: average outburst duty cycle during active intervals

^c: fraction of outbursts followed by dips

^d: References to detailed paper: (1) this work, (2) [Szkody et al. \(2013\)](#), (3) [Kato & Kojiguchi \(2022\)](#), (4) [Kato et al. \(2021\)](#), (5) [Simonsen et al. \(2014\)](#), (6) [Kato \(2019\)](#), (7) [Kato & Moriyama \(2022\)](#), (8) [Kato et al. \(2020\)](#), (9) [Mason & Howell \(2016\)](#), (10) [Lee et al. \(2021\)](#), (11) [Sun et al. \(2024b\)](#), (12) [Kato et al. \(2022\)](#), (13) [Gies et al. \(2013\)](#), (14) [Kimura et al. \(2020a\)](#), (15) [Sun et al. \(2024a\)](#)

mains open. The AH Pic syndrome may then be seen as an extreme manifestation of the IW And phenomenon.

6. DISCUSSION

Small scale stunted outbursts in novalike variables have long been known. Even the occurrence of long trains of such brightenings has been observed in at least one system (FY Per) already long ago ([Honeycutt 2001](#); [Honeycutt & Kafka 2004](#)). A second object with similar properties (KIC 9202990) was identified by [Østensen et al. \(2010\)](#) and [Ramsay et al. \(2016\)](#). Recently, yet another system (V1116 Cep) has been recognized to show a very similar behavior ([Shears 2020](#); [Shears & Bean 2023](#)). But no connexion between the three stars was established. However, with four more NLs (CM Del, AH Pic, V2837 Ori and PS Eri) exhibiting the same phenomenon, distinct from almost all other systems known to suffer stunted outbursts, and with

other strikingly similar characteristics, in particular the almost identical orbital waveforms, it is appropriate to look for a common origin for this behavior.

The question is thus: what causes the quasi-periodic brightenings and why are they only observed in a minority of NLs? The answer will only be possible after the mechanism leading to stunted outbursts in the first place is identified. Only then more specific details such as the cause for the slow evolution of outburst intervals and profiles, and their correlation, or the reason for the temporary suspension of the outburst activity can be addressed. It appears that we are still far from understanding this phenomenon. Already early-on [Honeycutt et al. \(1998\)](#) discussed arguments in favour of possible mechanisms, as well as their problems. These mechanisms can basically be divided into two categories, namely (1) modulation of the mass transfer rate from the secondary star, and (2) disk instabilities similar to those leading to

dwarf nova outbursts, also considering truncated accretion disks and Z Cam-like outbursts. However, for none of the scenarios a more specific mechanism has convincingly been proposed. The lack of a more detailed understanding of the underlying physics is discussed by Hameury (2020). Subsequently, I will regard in some more detail the arguments in favour and the problems of the two scenarios with particular emphasize on the AH Pic syndrome.

6.1. *Disk instabilities*

Ordinary dwarf nova outbursts have extensively been investigated within the DIM theory (see Lasota 2001, for a thorough review). Even if many questions concerning specific aspects are still open, quasi-periodic outbursts, including events occurring in quick succession, have routinely been simulated. Were it not for the small amplitude, the outburst behavior of the AH Pic stars would not be unlike that of dwarf novae such as CN Ori which has a very high duty cycle as evidenced by its ASAS-SN light curve.

One of the problems often mentioned in this context concerns the average mass transfer rate \dot{M} from the secondary. In order for the DIM to work it must be below a given threshold \dot{M}_{crit} . However, novalike variables are generally supposed to have a high \dot{M} which keeps the accretion disk in a permanent high state not unlike dwarf novae during outbursts. Could it be that systems with stunted outbursts and in particular the AH Pic stars have mass transfer rates close to \dot{M}_{crit} so that disk instabilities are still enabled? For none of the AH Pic stars \dot{M} has been measured. But their absolute magnitude may serve as a rough proxy. As shown in Fig. 11 they are all in the range where the distribution function of NLs and dwarf novae overlap. This may be an indication that the mass transfer rate through their disks is within the range that still permits disk instabilities and dwarf nova outbursts.

But then, the likelihood for stunted outbursts to occur should be enhanced when the overall brightness of the system is reduced, that is, when the average mass transfer rate is smaller. However, Honeycutt (2001) concludes that there is no correlation between the occurrence of stunted outbursts and the system brightness either in a given system or from system to system. Moreover, two distinct minima can be seen in the long-term light curve of V1116 Cep (Fig. 2), one close to JD 2456000, the other around JD 2457750. During both events outbursts are suppressed. Similarly, during the low state of the candidate system V794 Aql the outburst activity is at least temporarily suspended. There may thus be a tendency for stunted outbursts to occur when the overall system

brightness is higher. This goes in the wrong direction if stunted outbursts were to be explained within the DIM scenario.

Honeycutt et al. (1998) raised the hypothesis that stunted outbursts are just like normal dwarf novae outbursts but seen against an attenuating background light source. Honeycutt (2001) discussed this idea further. He compared the amplitude distribution of stunted outbursts with that of SS Cyg- and Z Cam-type dwarf novae derived from compilations of Warner (1995a) and found the best congruity if the diluting light source is 3.5 mag (or 25 times) brighter than the outbursting light source in quiescence. The data listed in Table A1 yield a mean outburst amplitude of 2.5 ± 1.0 mag, somewhat less than the center of the distribution used by Honeycutt (2001). Together with the mean amplitude of the outbursts of the AH Pic stars of 0.74 ± 0.18 mag the constant light should then on average be 8.4 times (2.3 mag) brighter than the variable light at minimum. Thus, the contrast between the two light sources needs not to be as drastic as the 3.5 mag found by Honeycutt (2001). But still, although Honeycutt (2001) briefly mentions some possible scenarios it is not obvious where the diluting light should come from.

Another hypothesis discussed by Honeycutt et al. (1998) concerns the idea that small amplitude outburst caused by the DIM mechanism may be possible if the accretion disk is truncated and the inner parts of the disk are missing. A disk may be truncated for different reasons. The most widely investigated possibility is a disruption of the inner disk by the strong magnetic field in intermediate polars. In that case a light curve modulation on time scales of minutes is most often visible, revealing the rotation period of the white dwarf. This effect is easily detected in TESS light curves (Bruch, in preparation), but it is not seen in the TESS data of any of the AH Pic stars. Therefore, a disk truncated by a white dwarf magnetic field cannot explain the AH Pic syndrome, even more so considering that outbursts in truncated disks are supposed to be infrequent, as Honeycutt et al. (1998) pointed out.

Dwarf nova outbursts occur semi-periodically. While this is also the case for the AH Pic stars, it is not so for the majority of stars exhibiting stunted outbursts where the brightenings occur quite irregularly or only sporadically, sometimes in small clusters separated by long intervals without outburst activity. Thus, if stunted outbursts are indeed caused by disk instabilities, an explanation for the quite distinct outburst pattern in AH-Pic stars and in other novalike variables is required.

6.2. *Mass transfer variations*

An alternative explanation for stunted outbursts are mass transfer bursts from the secondary star. Some observations appear to favor this mechanism, but there are also problems.

Baptista et al. (2011), using eclipse mapping techniques, find that the behavior of UU Aqr during a stunted outburst is incompatible with the disk instability model for dwarf nova outbursts and therefore prefer modulations of the mass transfer to explain the brightenings. While this is not a direct argument in favor of mass transfer variations, Robertson et al. (2018) defend this notion even more emphatically. The principle diagnostic tool is the hot spot, that is, the region where the stream of transferred matter hits the accretion disk edge. Variations of the mass transfer rate should lead to a modulation of the brightness of the hot spot, and – in eclipsing systems – to variations of the eclipse shape and the minimum phase. Robertson et al. (2018) analysed eclipse profiles in UU Aqr during stunted outbursts and found in about half of them hot spot enhancements and a delayed eclipse egress. They take this as evidence for increased mass transfer. They hypothesize that the absence of such signatures in the remaining eclipse profiles may be due to blobby mass transfer, such that the stream of matter is not constant on the orbital time scale.

A change of the eclipse profiles as a function of the outburst phase is also evident in the two eclipsing AH Pic stars CM Del and KIC 9202990 (Fig. 12). In a symmetrical accretion disk the light center will coincide with the disk center and thus the white dwarf location. A hot spot will shift the light center away from the disk center, and this effect will increase with the hot spot brightness. Moreover, the light center will become broader. Consequently, the eclipse profile will also broaden, and the minimum will be shifted in phase (to later phases because the hot spot is eclipsed after the disk center). In CM Del and KIC 9202990, a shift of 0.030 and 0.029, respectively, of the minimum phase is observed between the faint and bright outburst phases. Moreover, at least in KIC 9202990 the eclipse also appears to be broader during outburst maximum.

On the other hand, from Fig. 2 of Smak (1989) it can be estimated that a mass transfer enhancement of the order of 10 times is required for an increase of the disk brightness by 0.5 – 1 mag, typical for stunted outbursts. As Warner (1995b) pointed out, in dwarf novae (having fainter accretion disks than novalike variables but similar secondary stars) mass transfer modulations of this magnitude would cause strong variations of the hot spot brightness which are not observed on time scales of stunted outbursts. This constitutes a prob-

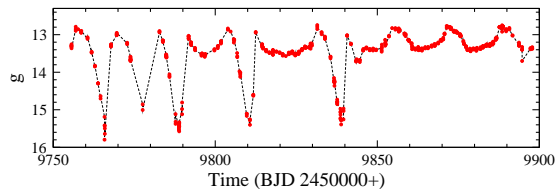


Figure 16. Detail of the ASAS-SN light curve of PS Eri containing dips and the transition to the normal outburst behavior.

lem for scenarios to explain stunted outbursts by mass transfer variations from the secondary stars. Moreover, concerning the AH Pic syndrome, a mechanism would be required to drive such variations over years semi-periodically on time scales of week. I am not aware of such a mechanism. The rather exotic idea that a third body in an eccentric orbit around the central binary system may induce slight variations of the Roche lobe size of the secondary star and thus variations of its atmospheric scale height at the L_1 point, causing the mass transfer to increase and decrease, can be refuted because this effect would be strictly periodic, while the outburst intervals in AH Pic stars are not stable.

6.3. Dips

An enigmatic feature associated with stunted outbursts are brightness dips which occur occasionally right after the end of the outburst. This happens in systems with sporadic outbursts (Honeycutt et al. 1998; Honeycutt 2001) as well as in some AH Pic stars (CM Del: Fig. 4; AH Pic: Fig. 1; KIC 9202990: Fig. 9) and is particularly evident in PS Eri (Fig. 6). There is a strong tendency for these events to cluster within limited time intervals. Such dips occur even more frequently in the anomalous Z Cam stars (see Sect. 5.2), but dip clustering is much less evident in these systems. An amplified section of the ASAS-SN light curve of PS Eri containing some dips and the transition to the normal outburst behavior is shown Fig. 16.

During the dip intervals the total amplitude of the variations becomes similar to the average outburst amplitudes of dwarf novae. As a curious feature I note that, while the limited data sampling precludes a corresponding statement for the other dipping AH Pic stars, the dips (at least the last three dips in Fig. 16) in PS Eri appear not to occur after a stunted outburst, but interrupt the outburst. That is, the outburst is still in progress after recovery from the dip. I am not aware that this strange behavior has been observed before in a stunted outburst of any NL. But a similar effect can be identified in the ASAS-SN light curves of some IW And stars.

6.4. *Some basic statistics*

AH Pic stars appear not to be numerous. Based on his monitoring of NLs Honeycutt (2001) estimated that the fraction of novalike variables exhibiting stunted outbursts could approach 50%. His list of positive detections contains nine systems (not counting X Ser; see Sect. 5). Of 13 old novae observed by Vogt et al. (2018) six underwent such brightenings, leading to a similar fraction. Adding to these studies the list of Zsidi et al. (2023), 24 NLs exhibit stunted outbursts. None of these studies did specifically aim targets with continuous sequences of outbursts and thus should not be grossly biased towards such stars. Among the 24 systems only two are AH Pic stars (CM Del and FY Per). Taking these numbers at face value, a fraction of about $0.5 \times 2/24 \approx 0.04$ of all novalike variables are expected to be AH Pic stars. Acknowledging that I am dealing with small number statistics, this result should not be taken too seriously. However, it shows that the AH Pic stars are probably a small minority among NLs.

7. SUMMARY

New observational facilities in space and on Earth together with amateur astronomers having access to ever more sophisticated instrumentation has enabled close monitoring of many variable stars during the past one or two decades to a degree that was unthinkable previously. Light curves with no or few interruptions extending over years, sometimes with a time resolution as short as a minute, enabled the detection of never before seen features. Among these are the phenomena studied in this paper.

Low scale brightenings in novalike variables lasting for a week or so have been observed before. But they were mostly seen as isolated events. The detection of long trains of such stunted outburst in close succession lasting for years required the new approach mentioned above. Of the seven stars identified to exhibit this behavior, four (V1116 Cep, CM Del, FY Per, and KIC 9202990)

were noted in the past to show this property. However, it was never discussed as a special feature and no connexion between the stars was established. The three additional systems presented here (AH Pic, V2837 Ori, and PS Eri), plus the detection of other common properties beyond the continuous stunted outbursts, namely the very similar stable orbital waveforms and their consistent variations during and between brightenings, and their absolute magnitudes in the overlap range between absolute magnitudes of NLs and dwarf novae above the CV period gap, justifies to regard them as a group. An understanding of this AH Pic syndrome has not yet been achieved. It requires in the first place the identification of the mechanism leading to stunted outbursts, and then an explanation for their continuous occurrence in AH Pic star, while they are seen only occasionally or not at all in the large majority of novalike variables. Only then more specific details of their behavior can be addressed,

This paper is based on data collected by the TESS and Kepler missions and obtained from the MAST data archive at the Space Telescope Science Institute (STScI). Funding for the missions is provided by the NASA Explorer Program and the NASA Science Mission Directorate for TESS and Kepler, respectively. STScI is operated by the Association of Universities for Research in Astronomy, Inc., under NASA contract NAS 5-26555. Further data collected by ASAS-SN are used. This project is funded in part by the Gordon and Betty Moore Foundation through grants GBFM5490 and GBFM10501 to the Ohio State University, and also in part by the Alfred P. Sloan Foundation grant G-2021-14192. Last not least, data downloaded from the AAVSO International Database contributed to this paper. I am grateful to all the individuals who keep these projects alive and to the many observers who supply data to the AAVSO archives. I also thank the anonymous referee for critical comments which led to an improvement of the original version of this paper.

APPENDIX

A. ABSOLUTE MAGNITUDE DISTRIBUTION FUNCTIONS

The distribution function of the absolute V magnitudes of SS Cyg and Z Cam type dwarf novae during quiescence and outburst maximum (i.e., avoiding the systematically fainter SU UMa and WZ Sge type stars) was calculated based on a sample of 89 systems with orbital periods above the CV period gap and below 10 h. The average apparent magnitudes were estimated in their ASAS-SN V band light curves. Together with their Gaia DR3 distances (Bailer-Jones et al. 2021) and the interstellar absorption, calculated using the E_{B-V} values taken from the compilation of Bruch & Engel (1994) or estimated from the tridimensional extinction maps (Stilism, Lallement et al. 2014; Capitanio et al. 2017) this yields the absolute magnitude. Since the magnitude depends on the orbital inclination a correction for this effect using

the formula of [Webbink et al. \(1987\)](#) was applied to all systems with known inclination. The latter were taken from the final edition (Dezember 2016) of the Ritter & Kolb catalogue ([Ritter & Kolb 2003](#)) or references cited therein. In a few cases of eclipsing systems without measured inclination a rough estimate based on the eclipse depth was made. The results are listed in [Table A1](#).

Table A1. Average apparent V magnitude during quiescence and outburst, distances, interstellar reddenings, orbital inclinations and average absolute V magnitudes for 89 SS Cyg- and Z Cam-type dwarf novae.

Name	m_V (qui)	m_V (outb)	Distance pc	E_{B-V}	Incl. ($^\circ$)	M_V (qui)	M_V (outb)
RX And	13.4	10.9	197	0.02	51	7.1	4.7
AR And	16.2	12.7	410	0.02	...	8.2	4.6
DX And	15.1	12.3	585	0.11	45	6.3	3.5
IW And	16.7	14.0	850	0.06	...	6.9	4.3
LX And	15.4	13.1	508	0.05	...	6.8	4.5
V823 And	14.9	14.0	469	0.08	80	5.1	4.2
VZ Aqr	16.6	12.9	598	0.03	...	7.7	4.0
UU Aql	16.3	11.7	306	0.13	41	9.0	4.3
FO Aql	16.1	13.9	514	0.06	...	7.5	5.3
PQ Aql	16.3	14.7	1388	0.07	...	5.4	3.9
V1101 Aql	15.2	13.9	687	0.05	...	5.9	4.7
AT Ara	14.3	12.4	783	0.12	38	5.0	3.0
SS Aur	14.6	11.2	249	0.05	38	7.9	4.6
Z Cam	13.1	10.5	213	0.02	57	6.5	3.9
AF Cam	16.9	13.6	874	0.32	...	6.3	3.0
SY Cnc	13.3	11.2	401	0.00	60	5.3	3.2
AT Cnc	14.7	12.7	455	0.03	...	6.4	4.5
GY Cnc	16.3	12.9	271	0.02	77	8.1	4.8
AM Cas	14.6	13.0	421	0.12	...	6.2	4.6
HL CMa	13.2	11.1	294	0.06	45	6.0	3.9
SV CMi	15.9	13.1	414	0.02	...	7.8	5.1
BV Cen	13.0	11.6	359	0.10	53	5.1	3.7
MU Cen	14.8	12.7	505	0.06	58	6.2	4.0
V442 Cen	15.6	12.0	343	0.15	...	7.6	4.0
WW Cet	13.5	11.2	218	0.03	48	7.0	4.7
ST Cha	15.5	13.6	690	0.21	...	5.8	3.9
TT Crt	15.8	13.3	532	0.03	...	7.2	4.6
SS Cyg	11.9	8.9	113	0.07	51	6.6	3.7
EM Cyg	13.3	12.3	356	0.03	67	5.2	4.2
V516 Cyg	16.3	13.9	722	0.48	...	5.6	3.2
V542 Cyg	17.7	13.9	1482	0.08	...	6.7	2.9

Table A1 *continued*

Table A1 (*continued*)

Name	m_V (qui)	m_V (outb)	Distance pc	E_{B-V}	Incl. ($^\circ$)	M_V (qui)	M_V (outb)
V792 Cyg	15.9	14.2	1302	0.10	...	5.1	3.4
V795 Cyg	16.3	13.5	656	0.06	...	7.2	4.3
V811 Cyg	14.7	13.6	513	0.05	70	5.6	4.5
EZ Del	16.5	15.0	1474	0.07	...	5.5	4.0
AB Dra	14.7	12.4	397	0.10	...	6.5	4.2
CG Dra	16.8	15.6	1332	0.04	...	6.2	4.9
DO Dra	15.8	12.6	195	0.01	45	9.7	6.4
ES Dra	16.1	14.3	680	0.02	...	7.0	5.1
EX Dra	14.8	12.9	240	0.02	84	6.1	4.2
V416 Dra	16.7	14.2	595	0.06	...	7.7	5.2
AH Eri	17.6	14.4	1114	0.08	...	7.2	4.0
BF Eri	14.8	12.4	557	0.03	40	6.4	4.0
LT Eri	17.1	15.0	684	0.06	...	7.8	5.8
U Gem	14.2	9.4	93	0.04	70	8.9	4.1
AH Her	13.7	11.6	328	0.03	46	6.4	4.3
GY Hya	15.9	14.7	638	0.06	...	6.8	5.6
V495 Hya	18.0	14.1	1467	0.53	...	5.6	1.7
X Leo	15.9	12.2	438	0.00	41	8.2	4.4
HM Leo	17.2	13.4	506	0.03	...	8.7	4.9
IU Leo	15.4	13.0	749	0.03	...	6.0	3.7
RU LMi	16.6	14.4	927	0.02	...	6.8	4.7
CY Lyr	16.0	13.4	468	0.08	...	7.5	4.9
LL Lyr	17.3	13.7	827	0.05	...	7.7	4.1
V363 Lyr	17.7	15.8	1622	0.04	...	6.6	4.7
V584 Lyr	15.6	14.6	1011	0.10	...	5.3	4.3
CW Mon	16.5	12.5	326	0.02	...	9.0	5.0
V426 Oph	12.7	10.9	190	0.08	59	6.1	4.3
BI Ori	16.6	14.2	671	0.07	...	7.3	5.0
CN Ori	15.8	12.6	344	0.00	67	7.8	4.6
CZ Ori	16.2	12.5	500	0.00	24	8.3	4.7
BD Pav	15.0	12.8	328	0.06	71	6.7	4.6
GS Pav	17.0	14.8	531	0.04	79	7.3	5.1
RU Peg	12.1	10.3	274	0.04	33	5.4	3.6
HX Peg	15.3	13.1	586	0.25	...	5.8	3.6
IP Peg	14.8	12.3	140	0.01	84	7.3	4.9
V513 Peg	16.2	12.8	396	0.05	...	8.1	4.8
TZ Per	14.2	12.8	457	0.27	...	5.1	3.8
FO Per	16.2	13.5	588	0.00	...	7.5	4.8
KT Per	14.3	12.2	245	0.18	...	6.9	4.8

Table A1 *continued*

Table A1 (*continued*)

Name	m_V (qui)	m_V (outb)	Distance pc	E_{B-V}	Incl. ($^\circ$)	M_V (qui)	M_V (outb)
BV Pup	15.1	13.2	563	0.04	...	6.4	4.4
BX Pup	16.2	14.4	739	0.05	...	6.8	5.0
V729 Sgr	16.0	14.1	448	0.10	...	7.5	5.6
RY Ser	15.9	13.4	629	0.29	...	6.1	3.6
UZ Ser	16.4	12.9	306	0.25	...	8.3	4.8
VZ Sex	16.7	12.8	1498	0.03	...	5.8	1.9
TW Tri	16.3	15.6	684	0.06	...	7.1	6.3
CH UMa	15.1	10.8	374	0.02	21	7.8	3.6
TW Vir	16.9	12.2	400	0.03	43	9.2	4.5
HS 0218+3229	16.2	12.4	486	0.08	59	7.6	3.7
CRTS J044902.7-184129	16.9	14.4	898	0.03	65	6.9	4.4
CRTS J054558.3+022106	17.1	14.7	532	0.30	84	5.8	3.4
CRTS J064729.3+495027	16.4	13.3	1011	0.08	...	6.3	3.1
SDSS J090016.56+430118.2	17.9	14.4	852	0.03	...	8.3	4.7
CRTS J090210.2-113032	16.9	13.4	885	0.04	...	7.1	3.7
RX J1831.7+6511	16.6	14.2	854	0.04	...	6.9	4.6
CRTS J210846.4-035031	16.2	15.3	756	0.04	75	6.0	5.0
HS 2325+8205	16.6	14.0	464	0.12	...	8.0	5.4
Lanning 386	15.4	14.9	572	0.06	...	6.5	6.0

This approach contains several error sources. Flickering, orbital variations, insufficient data sampling, measurement errors and variations on long time scales all contribute to difficulties in defining the quiescent magnitude level in the ASAS-SN light curves which therefore is often uncertain by up to some tenths of a magnitude. Some light curves contain only few outbursts and due to the sampling of the observations the maximum may have been missed. The interstellar extinction also has considerable uncertainties, noting that in some cases the Stilism maps do not extend to the distance of the targets and thus provide only lower limits. Additionally, uncertain inclinations or the absence of a corresponding correction in the cases with unknown inclination contribute to errors of the absolute magnitude. Compared to these effects, distance errors introduce only moderate uncertainties. Note also, that no correction for the contribution of the secondary star was applied which may be substantial in the longer period systems. Overall, the individual absolute V magnitudes listed in Table A1 should be taken with a grain of salt. However, since most of the error sources are statistical and not systematic, they should cancel out in the ensemble average and thus not change substantially the distribution function of the absolute magnitudes.

The same holds true for the corresponding distribution function for novalike variables (which includes also old novae). In these cases the absolute V magnitudes were taken from Gilmozzi & Selvelli (2024) for 42 NLs and from Selvelli & Gilmozzi (2019) for 17 novae (excluding the long period system GK Per), noting that in the latter case the inclination correction was re-calculated using the Webbink et al. (1987) prescription.

The resulting normalized distribution functions are shown in Fig. 11 for novalike variables in solid black, and as solid red and dashed magenta lines for dwarf novae in quiescence and outburst maximum, respectively. They have distinct maxima, the average values being $M_V = 4.4 \pm 0.9$ (novalike variables), $M_V = 4.3 \pm 0.8$ (dwarf novae during outburst maximum) and $M_V = 6.9 \pm 1.1$ (quiescent dwarf novae). It is noteworthy that the distribution function of dwarf novae during maximum is remarkably similar to that of novalike variables.

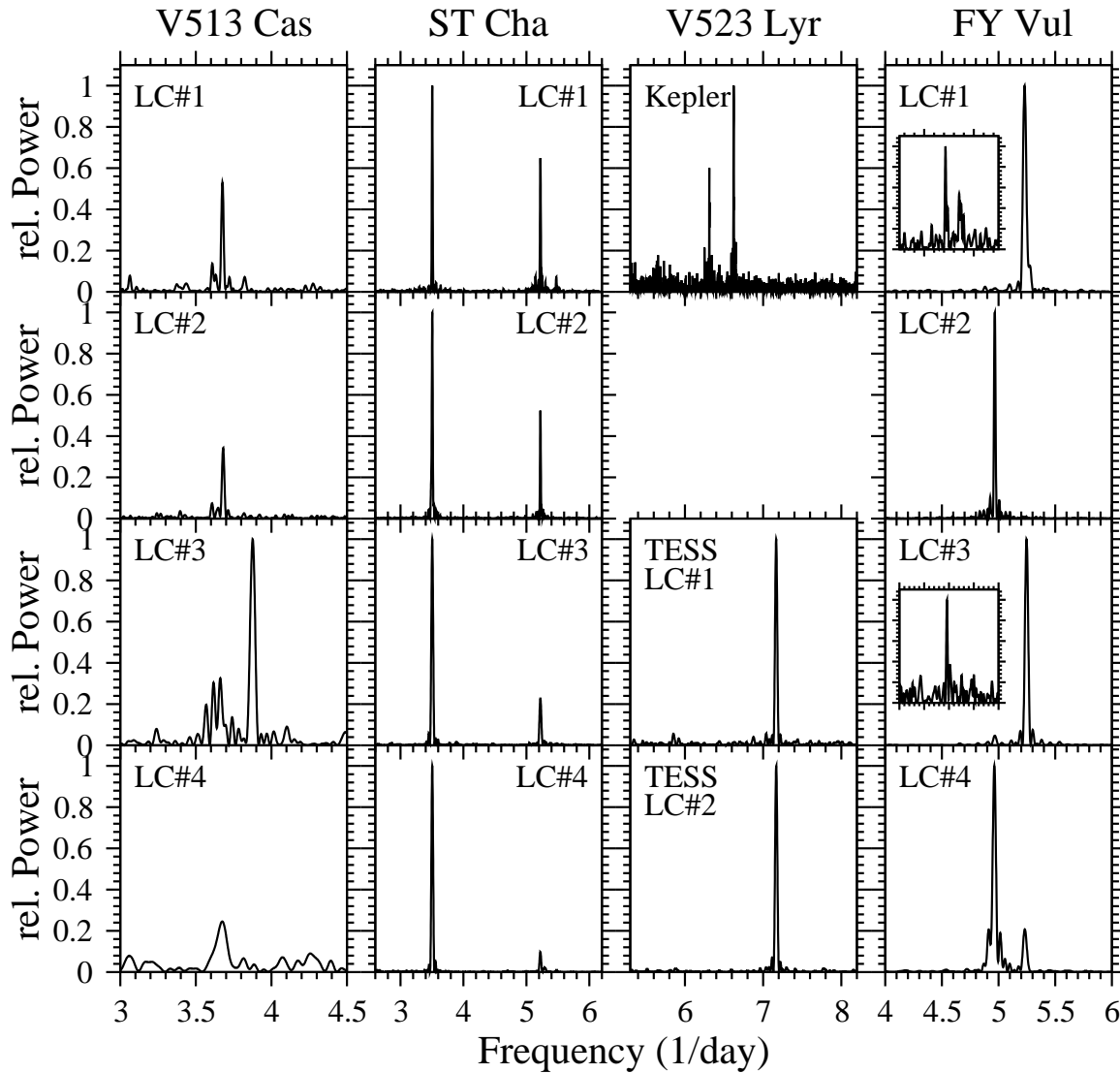


Figure A1. Power spectra of TESS and Kepler light curves of four systems with special features. For details, see text. The frequencies shown in the insets in the right column range between 14.5 and 16.5 d^{-1} .

B. FREQUENCY ANALYSIS OF SOME ANOMALOUS Z CAM STARS

The TESS light curves of some of the anomalous Z Cam stars discussed in Sect. 5.2 exhibit features in their power spectra that are either unusual or put into question previous understandings. Therefore, I briefly present them here without trying to investigate them in depth.

B.1. *V513 Cassiopeiae*

Szkody et al. (2013) determined a spectroscopic orbital period of V513 Cas of $P_S = 312 \text{ min} = 0.217 \text{ d}$. The power spectra of the four available TESS light curves are displayed in the left column of Fig. A1. In LC#1 and LC#2 a signal corresponding to an average period of $P_1 = 0.27186(8) \text{ d}$ is seen. It is not well defined in LC#3 which instead contains a strong signal at $P_2 = 0.2580(2) \text{ d}$. LC#4 encompasses only half of a TESS sector. Therefore, the spectral features are much broader and are ignored here. Considering that $1/P_S - 1/P_1 = 0.95 \approx 1$ it may well be that the spectroscopic period of Szkody et al. (2013) is a 1/day alias of the true orbital period P_1 . P_2 is then readily interpreted as being due to a negative superhump.

B.2. *V523 Lyrae*

In the Kepler light curve of V523 Lyr [Mason & Howell \(2016\)](#) identified two periodic modulations. The power spectrum of the entire light curve in the relevant frequency range is shown in the upper panel of the third column of Fig. A1. [Mason & Howell \(2016\)](#) interpret a persistent variation at 0.15845048 d as orbital, and a shorter one at 0.151 d, which is only visible during a short part of the light curve, as being caused by a negative superhump. None of these signals is seen in the two TESS light curves. Instead, the power spectra of both light curves have a strong signal at a higher frequency (lower panels of the third column of Fig. A1). The average corresponds to a period of 0.13953(2) d. I have no immediate explanation for the discrepancy between the periods detected in the Kepler and the TESS data. But V523 Lyr is a faint star located in a rich field. Keeping in mind the coarse pixel size of TESS contamination of the light curve by neighboring stars is therefore well possible.

B.3. *ST Chamaeleontis*

[Steiner et al. \(1988\)](#) first observed a photometric period of 6.85 hr or 0.285 d in ST Cha which they interpreted as orbital. This same period is consistently present in the power spectra of the four TESS light curves (second column of Fig. A1), permitting to refine it to 0.28532(3) d. However, all spectra contain another significant and stable signal, corresponding to a period of 0.19148(3) d. The relationship between the two periods is not obvious. Their large difference precludes to interpret them as a pair of orbital and superhump variations. ST Cha is quite bright in a poorly populated field so that contamination by neighboring stars is not an issue in this case.

B.4. *FY Vulpeculae*

The orbital period of FY Vul is unknown. The power spectra of four TESS light curves are shown in the right column of Fig. A1. Clearly, two different signals are present. The first one corresponding to a period of $P_1 = 0.20139(9)$ d is absent in LC#1, weak in LC#3 and strong in LC#2 and LC#4. The second one with a period of $P_2 = 0.1910(4)$ d is absent in LC#2, modestly strong in LC#4 and dominating in LC#1 and LC#3. It is close at hand to identify $P_1 = P_{\text{orb}}$ with the orbital period of FY Vul and $P_2 = P_{\text{nSH}}$ with the period of a nSH. Curiously, whenever the superhump is strong a weak signal is seen corresponding to period of $P_3 = 0.06475(9)$ d (insets in the corresponding panels in Fig. A1). Another structure to the right of this signal in LC#1 can be identified with the second overtone of the superhump frequency ($P_{\text{nSH}}/3$). While P_3 is clearly not an overtone of P_{orb} it is interesting to note that within the error margins the frequency difference $3/P_{\text{sh}} - 1/P_3$ is equal to the frequency difference $1/P_{\text{nSH}} - 1/P_{\text{orb}}$.

B.5. *LAMOST J065237.19+243622.1*

The periods exhibited by LAMOST J065237.19+243622.1 are confusing. In the Kepler K2 light curve [Sun et al. \(2024b\)](#) identified two periods at 0.15511 and 0.15419 d. The first (LC#1) of two TESS light curves contains a period of 0.16224(9) d. [Sun et al. \(2024b\)](#) interpret it as orbital and claim the presence of a second periodicity at 0.15659 d. The latter period and those seen in the Kepler data may indicate a nSH with a somewhat unstable period. The power spectrum is shown in the upper left panel of Fig. A2. The second TESS light curve (LC#2) was not yet available when [Sun et al. \(2024b\)](#) submitted their paper. Its power spectrum is shown in the upper right panel of the figure. Surprisingly, it is dominated by a broad feature, encompassing the period range between 0.150 and 0.164 d, and peaking at 0.1543 d. This range includes all previously seen periods. The broad feature is flanked by a narrow signal at 0.14440(3) d.

The time resolved power spectrum of LC#2, using a sliding window of 4 d width, sheds some light on this issue. It is reproduced in the lower panel of Fig. A2, while its middle panel contains the light curve on the same time scale. The broad feature in the power spectrum of the whole light curve is generated by a strong signal with rapidly changing frequency that only appears close to the end of the light curve concurrently with the maximum of a brightening of LAMOST J065237.19+243622.1. In contrast, the narrow signal, while weak, is persistent over its whole extend. While the complex behavior of the variations in the system warrants a deeper study than can be done here, I permit myself to speculate that the 0.14440 d period is the true orbital period (noting that in the power spectrum of LC#1 an otherwise inconspicuous peak is present at exactly the same frequency as in LC#2; see Fig. A2), while all other signals are due to a positive superhump with a somewhat variable frequency.

REFERENCES

- Armstrong, E., Patterson, J., Michelsen, E., et al. 2013, MNRAS, 435, 707
- Aungwerojwit, A., Gänsicke, B.T., Rodríguez-Gil, P. et al. 2005, A&A, 443, 995

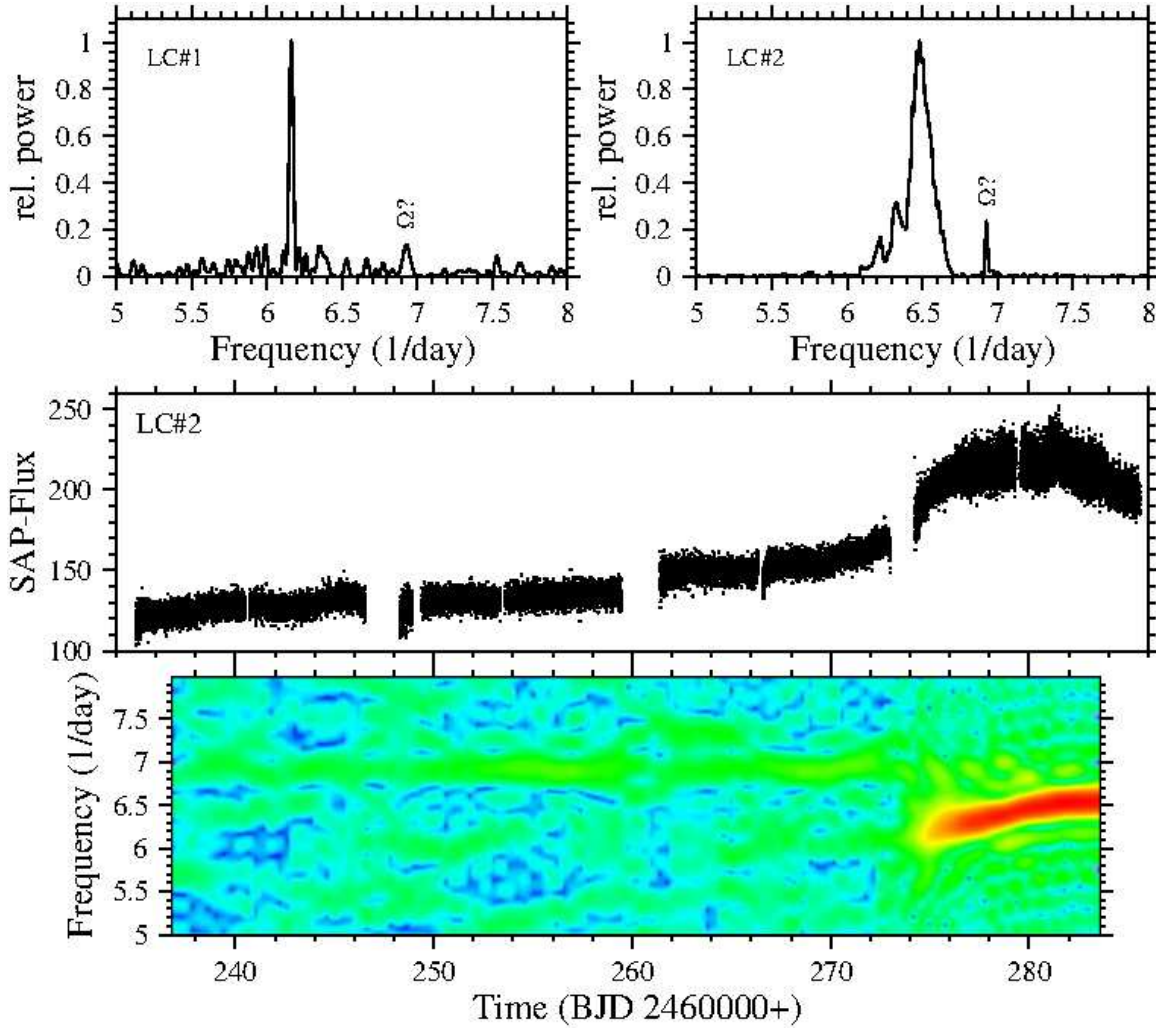


Figure A2. *Top:* Power spectra of the two TESS light curves of LAMOST J065237.19+243622.1. The tentatively identified orbital signals are marked as $\Omega?$ (see text). *Middle:* Light curve LC#2 of LAMOST J065237.19+243622.1. *Bottom:* Time resolved power spectrum of LC#2 on the same time scale. In order to enhance fainter features the power has been scaled to its fourth root.

Bailer-Jones, C.A.L., Rybizki, J., Fouesneau, M., Demleitner, M., & Andrae, R. 2021, *AJ*, 161, 147
 Baptista, R., Bortoletto, A., & Honeycutt, R.K. 2011, arXiv.1105.1381
 Bond, H.E. 1978, *PASP*, 90, 526
 Borucki, W.H., Koch, D., Basrik, G., et al. 2010, *Science*, 327, 977
 Bruch, A. 2017, *NewA*, 57, 51
 Bruch, A. 2019, *MNRAS*, 489, 2961
 Bruch, A. 2021, *RNAAS*, 5, 188
 Bruch, A. 2022, *MNRAS*, 509, 4669
 Bruch, A. 2023a, *MNRAS*, 519, 352
 Bruch, A. 2023b, *MNRAS*, 525, 1953
 Bruch, A. 2024a, *ApJS*, 273, 6
 Bruch, A. 2024b, *AJ*, 168, 121
 Bruch, A., & Engel, A. 1994, *A&AS*, 104, 79

Capitania, L., Lallement, R., Vergeley, J.L., Elyajouri, M., & Monreal-Ibero, A. 2017, *A&A*, 606, A65
 Chen, A., O'Donoghue, D., Stobie, R.S., Kilkenny, D., & Warner, B. 2001, *MNRAS*, 325, 110
 Drake, A.J., Djorgovski, S.G., Mahabal, A., et al. 2009, *ApJ*, 696, 870
 Downes, R.A., Hoard, D.W., Szkody, P., & Wachter, C. 1995, *AJ*, 110, 1824
 Downes, R.A., Webbink, R.F., Shara, M.M., et al. 2001, *PASP*, 113, 764
 Gies, D.R., Guo, Z., & Howell, S.B. 2013, *ApJ*, 775, 64
 Gilmozzi, R., & Selvelli, P. 2024, *A&A*, 622, A83
 Hameury, J.-M. 2020, *AdSpR*, 66, 1004
 Hameury, J.-M., & Lasota, J.-P. 2014, *A&A*, 569, A48
 Hoffmeister, C. 1963, *Astron. Nachr.*, 287, 169
 Honeycutt, R.K. 2001, *PASP*, 113, 473

- Honeycutt, R.K., & Kafka, S. 2004, AJ, 128, 1279
- Honeycutt, R.K., Kafka, S., & Robertson J.W. 2014, AJ, 147, 10
- Honeycutt, R.K., & Robertson, J.W. 1998, AJ, 116, 1961
- Honeycutt, R.K., Robertson, J.W., & Turner, G.W. 1998, AJ, 115, 2527
- Hümmrich, S., Bernard, K., & Srdoc, G. 2014, OEJVS, 167
- Hümmrich, S., Gröbel, R., Hamsch, F.-J., et al. 2017, New Astr., 50, 30
- Kafka, S. 2021, Observations from the AAVSO International Data Base available at <https://www.aavso.org>
- Kato, T. 2019, PASJ, 71, 20
- Kato, T., Kasai, K., Pavlenko, E.P., et al. 2022, arXiv:2202.11832
- Kato, T., & Moriyama, M. 2022, arXiv:2203.05143
- Kato, T., & Kojiguchi, N. 2020, PASJ, 72, 98
- Kato, T., Tampo, Y., Kojiguchi, N., et al. 2021, PASJ, 73, 1280
- Kato, T., Wakamatsu, Y., Kojiguchi, N., et al. 2020, PASJ, 72, 11
- Kimura, M., Osaki, Y., & Kato, T. 2020a, PASJ, 72, 94
- Kimura, M., Osaki, Y., Kato, T., & Mineshige, S. 2020b, PASJ, 72, 22
- Kochanek, C.S., Shappee, B.J., Stanek, K.Z., et al. 2017, PASP, 129, 104502
- Lallement, R., Vergeley, J.-L., Valette, J., et al. 2014, A&A, 561, A91
- Lasota, J.-P. 2001, NewAR, 45, 449
- Lee, C.-D., Ou, J.-Y., Yu, P.-C., et al. 2021, ApJ, 911, 51
- Lyons, K., Stys, D., Slevinsky, R., Sion, E., & Wood, J.H. 2001, AJ, 122, 327
- Mason, E., Howell, S.B. 2016, A&A, 589, 106
- Østensen, R.H., Silvotti, R., Charpinet, S., et al. 2010, MNRAS, 409, 1470
- Ramsay, G., Hakala, P., & Wood, M.A. 2016, MNRAS, 455, 2772
- Ricker, G.R., Winn, J.N., Vanderspek, R., et al. 2014, J. Astr. Tel. Instr. & Systems, 1, 014003
- Ritter, H., & Kolb, U. 2003, A&A, 404, 301
- Robertson, J.W., Honeycutt, R.K., Henden, A.A., & Campbell, R.T. 2018, AJ, 155, 61
- Robinson, E.L. 1976, ARAA, 14, 119
- Rodríguez-Gil, P., Schmidtobreick, L., & Gänsicke, B.T. 2007, MNRAS, 374, 1359
- Sazonov, A.V., & Shugarov, S.Yu. 1992, IBVS No. 3744
- Savitzky, A., & Golay, M.J.E. 1964, Analytical Chemistry, 36, 1627
- Schaefer, B.E. 2022, MNRAS, 517, 3640
- Selvelli, P., & Gilmozzi, R. 2019, A&A, 622, A186
- Shafter, A.W. 1985, AJ, 90, 643
- Shears, J. 2020, JBAA, 130, 234
- Shears, J., & Bean, S. 2023, JBAA, 133, 115
- Šimon, V. 2018, A&A, 614, A141
- Simonsen, M. 2011, JAAVSO, 39, 66
- Simonsen, M., Bohlens, T., Hamsch, F.-J., & Stubbings, R. 2014, JAAVSO, 42, 199
- Smak, J. 1989, AcA, 39, 317
- Steiner, J.E., Cieslinski, D., & Jablonski F.J. 1988, ASPC, 1, Progress and Opportunities in Souther Hemisphere Optical Astronomy, eds. V.M. Blanco & M.M. Phillips, (San Francisco, CA: ASP), 67
- Sun, Q.-B., Qian, S.-B., Zhu, L.-Y., et al. 2024a, arXiv:2409.03011
- Sun, Y., Li, X., Ao, Q., et al. 2024b, MNRAS, 531, 422
- Szkody, P. 1985, AJ, 90, 1837
- Szkody, P., Albright, M., Linnell, A.P., et al. 2013, PASP, 125, 1421
- Vogt, N., Tappert, C., Puebla, E.C., et al. 2018, MNRAS, 478, 5427
- Voges, W., Aschenbach, B., Boller, T. et al. 2000, IAUC, 7432
- Warner, B. 1976, IAU Symp. 73, Structure and Evolution of Close Binary Systems, ed. P. Eggleton, S. Mitton, & J. Whelan (Dordrecht, D. Reidel Publishing Company), 85
- Warner, B. 1995a, *Cataclysmic Variable Stars*, Cambridge University Press, Cambridge
- Warner, B. 1995b, Ap&SS, 230, 83
- Webbink, R.F., Livio, M., Truran, J.W., et al. 1987, ApJ, 314, 653
- Zsidi, G., Nixon, C.J., Naylor, T., Pringle, J.E., & Page, K.L. 2023, A&A, 679, L3